HHS Public Access

Author manuscript

Mol Microbiol. Author manuscript; available in PMC 2017 January 01.

Published in final edited form as:

Mol Microbiol. 2016 January ; 99(1): 88–110. doi:10.1111/mmi.13218.

Helicobacter pylori strains vary cell shape and flagellum number to maintain robust motility in viscous environments

Laura E. Martinez[1,2,**], **Joseph M. Hardcastle**[3,**], **Jeffrey Wang**[2], **Zachary Pincus**[4], **Jennifer Tsang**[5], **Timothy R. Hoover**[5], **Rama Bansil**[3,*], and **Nina R. Salama**[1,2,*]

[1]Graduate Program in Pathobiology, Department of Global Health, University of Washington, Seattle, WA 98195 USA

[2]Division of Human Biology, Fred Hutchinson Cancer Research Center, Seattle, WA 98109 USA

[3]Department of Physics, Boston University, Boston, MA 02215 USA

[4]Department of Developmental Biology and Department of Genetics, Washington University School of Medicine, St. Louis, MO 63110, USA

[5]Department of Microbiology, University of Georgia, Athens, GA 30602, USA

Summary

The helical shape of the human stomach pathogen *Helicobacter pylori* has been suggested to provide mechanical advantage for penetrating the viscous stomach mucus layer. Using single-cell tracking and quantitative morphology analysis we document marked variation in cell body helical parameters and flagellum number among *H. pylori* strains leading to distinct and broad speed distributions in broth and viscous gastric mucin media. These distributions reflect both temporal variation in swimming speed and morphologic variation within the population. Isogenic mutants with straight-rod morphology showed 7–21% reduction in speed and a lower fraction of motile bacteria. Mutational perturbation of flagellum number revealed a 19% increase in speed with 4 vs. 3 median flagellum number. Resistive force theory modeling incorporating variation of both cell shape and flagellum number predicts qualitative speed differences of 10–30% among strains. However, quantitative comparisons suggest RFT underestimates the influence of cell body shape on speed for helical shaped bacteria.

Keywords

Helicobacter pylori; cell shape; purified porcine gastric mucin; swimming speed; flagellar mutants; resistive force theory

[*]Corresponding Authors: Nina R. Salama, Fred Hutchinson Cancer Research Center, 1100 Fairview Ave. N, Mailstop C3-168, Seattle, WA 98109-1024, USA. Phone: 206-667-1540. Fax: 206-667-6524. nsalama@fhcrc.org. Rama Bansil, Department of Physics, Boston University, 590 Commonwealth Avenue, Boston, MA 02215, USA. Phone: 617-353-2969. Fax 617-353-9393. rb@bu.edu.

[**]L.E.M. and J.M.H. contributed equally to the research as first co-authors.

Competing interests: The author declares that no competing interests exist.

Author contributions

*L.E.M. and *J.M.H. contributed equally to the research as first co-authors; L.E.M. and J.M.H. conducted the experimental studies; J.W. helped with bacterial tracking analysis; and J.M.H. did the modeling. J.T., T.R.H., and Z.P. contributed new reagents/analytic tools; L.E.M. and J.M.H. analyzed data; and L.E.M., J.M.H., R.B. and N.R.S. designed the experiments, interpreted the results and wrote the paper.

Introduction

Cell shape diversification is suggested to be one mechanism that helps bacteria cope and adapt to different environments (Young, 2007). For the Gram-negative bacterium *Helicobacter pylori*, which colonizes the stomach of approximately half of the world's population, helical shape is thought to enhance motility through the highly viscous mucus overlying the gastric epithelium to which it adheres. Persistent colonization with *H. pylori* increases risk for gastroduodenal diseases including gastric and duodenal ulcers, gastric adenocarcinoma, and gastric B-cell lymphoma of mucosa-associated lymphoid tissue (MALT) (Peek and Crabtree, 2006; Wroblewski and Peek, 2013). As a neutrophile, *H. pylori* can survive only minutes in the stomach lumen (Schreiber *et al.*, 2004) and overcomes this acidic environment using urease, an enzyme that hydrolyzes urea to produce NH_3, locally elevating the pH to near neutral. Flagella-mediated motility is essential for infection in several species of pathogenic bacteria (Duan *et al.*, 2013). Successful colonization of the stomach by *H. pylori* requires both urease (Eaton *et al.*, 1991; Tsuda *et al.*, 1994a; Tsuda *et al.*, 1994b; Nakamura *et al.*, 1998), and flagella-mediated, chemosensory-directed motility (Eaton *et al.*, 1996; Terry *et al.*, 2005; Howitt *et al.*, 2011; Rolig *et al.*, 2012). Furthermore, urease activity may be directly relevant to motility.

Our earlier study showed that *H. pylori* is immobile in a purified porcine gastric mucin (PGM) gel at low pH, although flagella could be seen rotating (Celli *et al.*, 2009). Upon addition of urea, the bacteria became mobile (Celli *et al.*, 2009) because the hydrolysis of urea elevates the pH triggering a transition of PGM from a soft viscoelastic gel to a viscous solution (Celli *et al.*, 2005; Celli *et al.*, 2007). These experiments suggest that the helical shape of *H. pylori* does not help it bore its way like a corkscrew through the gel-like mucus layer of the stomach, as had been previously proposed (Yoshiyama and Nakazawa, 2000; Montecucco and Rappuoli, 2001). However, could the helical shape enhance the swimming of *H. pylori* in viscous solutions of PGM?. To the best of our knowledge, this question has not been examined by systematically comparing the motility of helical and rod-shaped mutants of the same species of bacteria.

From a hydrodynamics viewpoint, the shape of a swimmer is known to alter translational and rotational drag on the cell body, which can affect swimming speed and the bacterium's ability to sense chemotactic gradients in different environments (Dusenbery, 1998). Berg and Turner suggested that a helical cell shape would result in additional corkscrew-like propulsion for bacteria moving in viscous environments (Berg and Turner, 1979). Ferrero and Lee observed that in highly viscous methylcellulose (MC) solutions of varying viscosity (>100 cP), different clinical strains of helical-shaped *Campylobacter jejuni* were more motile than rod-shaped bacteria from several different species, *Vibrio cholerae*, *Salmonella enteritidis*, and *Escherichia coli* (Ferrero and Lee, 1988). Karim *et al.* showed that *H. pylori* and *C. jejuni* swim faster in liquid broth as compared to *E. coli,* presumably due to their helical cell body shape (Karim *et al.*, 1998). However, both these studies compare different species of bacteria, which have differences in flagellum morphology, number and arrangement, and possibly motor output, making conclusions on the influence of cell body shape difficult to interpret.

We and others approached the role of *H. pylori's* cell shape in stomach colonization using genetic screens to identify cell shape-determining (*csd*) genes required for *H. pylori's* characteristic helical cell morphology (Sycuro *et al.*, 2010; Bonis *et al.*, 2010; Sycuro *et al.*, 2012; *Sycuro et al.,* 2013). *H. pylori* cell shape mutants show impaired stomach colonization in a mouse infection model, suggesting helical cell shape is important for initial colonization and/or persistence in the stomach (Sycuro *et al.*, 2010; Bonis *et al.*, 2010; Sycuro *et al.*, 2012). Several *csd* genes encode peptidases that modify the bacterial cell wall, composed of peptidoglycan (PG), which is responsible for rigidity and cell shape in most bacteria (Cabeen and Jacobs-Wagner, 2005). Elimination of the PG peptidases Csd4 or Csd6 yielded bacteria with straight rod morphology, but the mutants show normal flagellation and cell growth properties (Sycuro *et al.*, 2012; *Sycuro et al.,* 2013). While we had previously shown a semi-solid agar motility defect for *csd4* straight rod mutants (Sycuro *et al.*, 2012), another group suggested that *csd6* mutants (*H. pylori* strain G27) show enhanced motility in semi-solid agar as compared to wild-type (Asakura *et al.*, 2010), but the morphology of the *csd6* mutant was not assessed. In *Campylobacter jejuni*, deletion of *pgp2,* a homolog to *H. pylori csd6*, results in straight rod morphology and mutants show motility defects in semi-solid agar, defects in biofilm formation, and reduced fitness in a chick colonization model (Frirdich *et al.*, 2014).

Here, we present a detailed study relating morphology and motility using optical and electron microscopy to measure cell shape and flagellum parameters, and live-cell imaging to track individual bacteria to examine swimming behavior in several polymer solutions including the physiologically relevant porcine gastric mucin (PGM). PGM is homologous to the human glycoprotein MUC5AC, the major secreted mucin expressed in the stomach mucosa by surface epithelial cells (Sellers *et al.*, 1987; Bansil *et al.*, 2013). PGM has been shown to exhibit similar rheological properties to human mucus scraped from the surface of the gastric mucosa, making it an ideal comparison to *H. pylori's* niche environment (Schrager and Oates, 1974; Pearson *et al.*, 1980; Bell *et al.* 1984; Bell *et al.*, 1985). Gastric mucus is believed to have two layers differing in mucin concentration, a thin firmly adherent, high concentration layer (around 30 mg mL^{-1}), and an overlying loosely adherent layer of mucus on the luminal surface (15 mg mL^{-1}) (Taylor *et al.*, 2004). We provide further insight into the effects of cell body shape morphology and flagellum number on *H. pylori* swimming speed using a resistive force theory model (Gray and Hancock, 1955). Combined experimental and theoretical findings indicate that *H. pylori's* natural variation in cell body shape and flagellum number independently contribute to robust motility in viscous environments, including gastric mucin.

Results

Gastric mucin shows physiologically relevant solution and gel-like properties

To examine the micro-rheological properties of the environment in which *H. pylori* motility is to be measured we used microscopic single particle tracking. This technique probes the Brownian motion of particles (for a review see Cicuta and Donald, 2007) and has been previously applied to investigate the microrheology of PGM (Lieleg *et al.*, 2010; Bansil *et al.*, 2013; Georgiades *et al.*, 2014). To model the viscous environment of the human gastric

mucosa where *H. pylori* resides, we used physiologically relevant concentrations of PGM of 15 and 30 mg mL^{-1}. For comparison to previous work on *H. pylori* motility in viscous solutions (Hazell *et al.*, 1986; Worku *et al.*, 1999), we also examined methylcellulose solutions at concentrations of 10 and 15 mg mL^{-1}. Fig. 1A shows the averaged mean squared displacement (MSD = $\langle r(t)^2 \rangle$, μm^2) of 1μm diameter fluorescent polystyrene particles calculated from the measured position ($r(t)$) as a function of time (t). To confirm that bacteria experience a similar environment, we also tracked Δ*motB* mutants, which retain wild-type flagellum structure but have non-functional flagellum motors (Ottemann and Lowenthal, 2002) (Fig. 1B). We found that the MSD values of non-motile bacteria were smaller relative to those acquired for diffusing particles (Fig. 1B). This reflects the increased drag due to the larger size and anisotropic shape of bacteria compared to spherical particles. The time dependence of the MSD is usually described using the relation $\langle r(t)^2 \rangle = At^{\alpha}$. In a viscous fluid, particles exhibit normal Brownian diffusion with the exponent $\alpha = 1$ and $A = 4D$, where A is the constant of proportionality and D is the diffusion constant of the particle (Cicuta and Donald, 2007). In complex fluids, such as viscoelastic gels, particles exhibit sub-diffusive behavior with an exponent of $\alpha < 1$.

By fitting the ensemble averaged MSD, we obtained the exponent α and A. For each solution, the values of α were the same for both polystyrene particles and Δ*motB* bacteria (Fig. 1C). Brownian diffusion ($\alpha = 1$) was observed in broth, PGM at 15 mg mL^{-1}, and MC solutions of 10 and 15 mg mL^{-1}, implying these solutions behave as viscous liquids (Fig. 1C). The viscosities (η) (cP) of each solution were calculated from the measured bead diffusion constants via the Stokes Einstein relation ($\eta = kT/6\pi RD$), where T and R represent temperature and bead radius, respectively (Fig. 1C). Sub-diffusive behavior was observed for PGM at 30 mg mL^{-1} ($\alpha = 0.65 +/- 0.10$), implying that at this higher concentration, PGM is a gel-like viscoelastic polymer (see Bansil *et al.*, 2013 for a brief review of viscoelasticity). Our results are in agreement with the observations of Georgiades *et al.*, where a transition to viscoelastic behavior was observed in PGM at 25 mg mL^{-1} (Georgiades *et al.*, 2014). Our results suggest that PGM at 30 mg mL^{-1} displays gel-like properties that resemble the rheological gel-like environment of mucus near the gastric epithelium, and PGM at 15 mg mL^{-1} displays solution-like properties that resemble the rheological environment that *H. pylori* encounters as it swims through the gastric mucus found near the acidic lumen of the stomach (Taylor *et al.*, 2004). We used these PGM concentrations in our *in vitro* experiments to model the solution and gel-like environments of stomach mucus and to examine *H. pylori* motility.

Wild-type H. pylori strains display diverse and distinct cell body and flagellum morphologies

To address the impact of cell morphology on motility, we began by analyzing the morphology of three unrelated wild-type strains: LSH100, B128, and PMSS1 (Table S1). *Helicobacter pylori* clinical strains show a high degree of genetic and phenotypic variability and there is no consensus lab strain used by the *H. pylori* research community. These commonly used strains were all isolated from symptomatic human patients on three different continents (PMSS1-Australia, LSH100-Europe, B128-North America) and robustly colonize mice (LSH100, PMSS1, B128) or mongolian gerbils (B128), the major small animal models

of *H. pylori* stomach infection. Cell morphology was characterized by analyzing phase contrast images using the CellTool software (Pincus and Theriot, 2007; Lacayo *et al.*, 2007; Sycuro *et al.*, 2010), which has been previously used to segregate *H. pylori* cells based on different shape parameters, including cell length, diameter, and side curvature (Sycuro *et al.*, 2010; Sycuro *et al.*, 2012; Sycuro *et al.* 2013). Side curvature is the measure of the total curvature of a bacterial cell excluding its poles and the curvature itself is defined as the reciprocal of the radius of a circle that is tangent to a curve made at any point (Sycuro *et al.*, 2010). Wild-type *H. pylori* strains display heterogeneous morphologies ranging from straight to predominantly helical, and bacterial cells of different cell lengths were observed within each population (Fig. 2A). As summarized in Table 1, all three strains have similar values of cell diameter but distinct cell length and side curvature profiles.

To further characterize helical morphology, we obtained the helical radius (R) and pitch (P) (length of one complete helical turn) using centerline measurements provided by CellTool. For each bacterial cell, centerlines were fitted using a sine function $y=Rsin\left(\frac{2\pi}{P}x+\delta\right)$ (Fig. 2B). Figures 2C–E show the distribution of each strains' cell length, helical radius, and helical pitch, and their average values are summarized in Table 1. All strains showed overlap in cell length distributions, but the B128 population shows a higher probability of shorter cells (Fig. 2C). PMSS1 showed an increased helical pitch as compared to both LSH100 and B128 (Fig. 2E), while LSH100 showed significantly increased helical radius as compared to both B128 and PMSS1 (Fig. 2D and Table 1). These observations correlated well with LSH100 having increased side curvature (Fig. 2A and Table 1), while B128 and PMSS1 showed smaller values consistent with a smaller radius.

We also examined flagellum morphologic parameters using transmission electron microscopy (TEM) and scanning electron microscopy (SEM) (see Experimental Procedures). The three wild-type strains showed a mixed population of cells with 0 to 6 unipolar flagella (Fig. 2F). LSH100 and B128 shared a median flagellum number of 3 +/− 1 (+/− standard deviation), while PMSS1 had a median flagellum number of 4 +/− 1 and a higher proportion of bacteria with 4 to 6 flagella (55%) relative to LSH100 (34%) and B128 (36%) (Fig. 2F). LSH100 had a median flagellum length of 3.4 +/− 0.3 μm, which was shorter than both PMSS1 (4.4 +/− 0.3 μm) and B128 (4.4 +/− 0.4 μm) (Fig. 2F).

In summary, the three wild-type *H. pylori* strains examined varied in multiple cell morphologic parameters expected to influence motility, including cell length (B128 shortest), helical radius (LSH100 highest), flagellum number (PMSS1 highest), and flagellum length (LSH100 shortest).

Wild-type H. pylori strains display a broad distribution of swimming speeds

To examine *H. pylori* motility, we used live-cell imaging and particle-tracking methods to automatically track hundreds of individual bacterial cells in broth and in viscous PGM or MC media. We collected videos of bacteria swimming at the mid-level plane between the coverslip and the glass slide. We tracked bacteria from ten second videos, which allowed us to capture bacteria swimming in the field of view and it provided sufficient time to acquire a broad sampling of each bacterium's instantaneous swimming speeds (Fig. S1). The recorded videos show that *H. pylori* exhibits a complex motion consisting of periods of straight

swimming (runs), interrupted by short periods of directional reorientation and/or reversal in swimming direction (see Video 1). Figure 3A shows a representative bacterial trajectory and Fig. 3B shows its corresponding instantaneous speed as a function of time. The speed is observed to vary between high values (~ 10 – 15 μm/s) and low values of ~ 1 μm/s. The low speeds show a one to one correspondence with reorientation events represented by a large change in swimming direction ($\Delta\theta$) as shown in Fig. 3C. Using a similar method to Son *et al.* (Son *et al.*, 2013) we classified reorientations as any event where abrupt decreases in bacterial swimming speed ($v_{local\ min} < (v_{avg}/2)$) happened or $\Delta\theta$ was significantly larger than angle changes resulting from rotational diffusion ($\Delta\theta > 25$ degrees was used exclusively in this study). Reversals were classified as any reorientation event for which the directional angle change $\Delta\theta > 110$ degrees (Fig. 3A). In our analysis, the direction of swimming observed at the start of the video was considered “forward” solely as an annotation relevant to the video frame and not relative to bacterial polarity. Polarity could not be determined because bacterial flagella were not observable at the magnification and optical resolution of our experiments. After a reversal occurred, bacteria were assumed to swim in the reversed direction until another reversal event took place. Using these criteria, all trajectories were segmented into forward and reverse swimming directions and reorientation events. From the segmented trajectories, we calculated several motility parameters: instantaneous swimming speeds (the speed between two points of a track); reversal frequency (reversals per second) and speed measurements of both forward and reverse directions; and percent track linearity (%TL, the ratio of average straight line velocity (μm/s) to average swimming speed (μm/s) x 100%). Measurements acquired during reorientation events were excluded from our speed calculations.

As shown in Fig. 4A–C, the three wild-type *H. pylori* strains exhibited broad overlapping distributions of instantaneous swimming speeds in broth and PGM. These distributions are concatenations of instantaneous swimming speeds from all bacterial cells analyzed for each strain and in each solution tested. The shapes of these broad speed distributions depend on both strain and medium in a complex way, presumably reflecting the differences in cell shape, number of flagella, and flagellum length. To characterize such broad distributions it is not enough to use a single average. We therefore computed the average speed (v_{avg}), median speed (v_m), maximum speed (v_{max}), and standard deviation (σ) of the distribution of speeds (Table 2). The maximum swimming speed gives a measure of the fastest swimming speed, likely arising when all flagella motor are firing in synchrony.

First considering LSH100 and PMSS1, Fig. 4A–C shows that LSH100 speed distributions are different from those of PMSS1, having lower speeds than PMSS1 in all three solutions. For example, in all three solutions v_{avg} and v_m are almost twice as large for PMSS1 compared to LSH100 and the standard deviation is approximately 30–40% larger (Table 2). Although v_{avg} of LSH100 and PMSS1 does not vary much between broth and PGM, these strains show increased proportion of higher swimming speeds in PGM compared to broth. This observation is also confirmed by the change in v_m. For LSH100 we find $v_m = 5.7$ μm/s in broth, which increases to 6.5 μm/s in PGM at 15 mg mL^{-1}, and exhibits a similar median swimming speed of 6.4 μm/s in PGM at 30 mg mL^{-1} (Table 2).

B128 shows similar speed distributions to LSH100 in broth and PGM at 30 mg mL^{-1} (Fig. 4A,C), while its speed distribution shifts to higher speeds in PGM at 15 mg mL^{-1}, becoming more similar to PMSS1 (Fig. 4B). This may be attributed to that fact that the shape of B128 is similar to PMSS1 but its flagellum parameters are closer to those of LSH100 (Fig. 2F). B128 also exhibits the non-monotonic trend in PGM observed for LSH100 and PMSS1 (Table 2).

In addition to monitoring the speed of swimming bacteria, we also recorded the number of bacteria that appeared non-motile for LSH100 and PMSS1 in broth and PGM. Bacteria that exhibited displacements < 0.3 μm were classified as non-motile (immobile). The percentage of immobilized bacteria in all solutions (10–50%) exceeded the percentage of bacteria with zero flagella (4–9%), and increased with increasing viscosity of the media (Table 3). PMSS1 had the fewest percent-immobilized bacteria and the highest v_m in all solutions. Thus, the tendency to not be immobilized in the viscoelastic PGM gel correlates with swimming speed.

Speed distributions also reflect temporal variation of individual bacteria

The speed distributions shown in Fig. 4 arise from two unrelated factors: (i) variation in bacterial cell shape and size in the population, and (ii) variation in the swimming speed of individual bacteria over time. As seen in Fig. 3B, individual bacteria alter their swimming speed by an order of magnitude over the time of tracking (typically 1–10 seconds). This temporal variation cannot result from variation in cell morphology, which should remain constant during the track time (*H. pylori* doubling time is 2.5 – 4 hours, depending on the strain, under these growth conditions). In order to separately assess the temporal variation we processed the trajectories of each bacterium and obtained the standard deviation of each bacterium's speed, σ_{bac}. Figure 4D shows the distribution of speed standard deviations, σ_{bac}, for the three different *H. pylori* strains in PGM at 15 mg mL^{-1}. The breadth of the σ_{bac} distributions (4D) indicate that population level speed variation (4B) is largely due to speed variation within individual bacterial trajectories (as illustrated for an example bacterium in Fig. 3B). LSH100, B128, and PMSS1 showed slightly different distributions (K-S statistics, $p < 0.05$ for all comparisons) suggesting they may have different swimming dynamics in PGM (Fig. 4D). We obtained similar results when comparing LSH100 to B128 and PMSS1 to B128 in PGM in 30 mg mL^{-1} (Fig. S2), although these differences were not observed when comparing LSH100 to PMSS1 in PGM 30 mg mL^{-1} (K-S, $p = 0.89$). Interestingly, all wild-type strains showed similar distributions in broth (K-S, $p > 0.05$) (Fig. S2). These results indicate that the temporal variation in swimming speeds of *H. pylori* depends on both the strain and swimming environment, and the breadth of the speed distribution is largely due to individual bacteria varying their swimming speed in time.

Helical cell shape promotes increased motility in broth and viscous media

To directly address whether the helical cell shape of *H. pylori* impacts its motility, we compared the motility of helical wild-type bacteria to isogenic straight rod mutants (Δ*csd6*) of LSH100 (see Videos 1–2). We first confirmed that the cell shape mutant did not show altered flagellum number or length (Table 4 and Fig. S3), as previously described (Sycuro *et al.*, 2012). We found that while the overall speed distribution of the LSH100 Δ*csd6* mutant

was similar to wild-type LSH100 in broth (Fig. 5A), v_m decreased by 7% (Table 2). In addition, straight rods displayed an 11% reduction in v_m in PGM at 15 mg mL^{-1}, and an 8% reduction in v_m in PGM at 30 mg mL^{-1} (Table 2). While the reduction in speed between the Δ*csd6* mutant and wild-type is statistically significant in the PGM solutions (K-S, p <0.0001), it is not so in the broth solution (K-S, p =0.0955) (Table 2).

To further test the generality of this phenomenon, we generated a *csd6* deletion mutant in the PMSS1 strain background. We first analyzed the cell shape of this strain and found that deletion of *csd6* resulted in straight rod morphology, measured as loss of cell curvature (Fig. S4), as previously shown in LSH100 (Sycuro *et al.*, 2013). The PMSS1 Δ*csd6* straight rod mutant also had normal flagellum number and length compared to wild-type (Table 4 and Fig. S3). In this case, we found significant differences between Δ*csd6* mutant and wild-type speed distributions in broth and in viscous PGM solutions (Fig. 5B), with a slightly larger reduction in median swimming speed compared to LSH100 (Table 2). For example, straight rods displayed an 11% reduction in v_m in broth and in PGM at 15 mg mL^{-1}, and a 13% reduction in a gel-like PGM environment at 30 mg mL^{-1} (Table 2).

To investigate whether straight rods exhibited reduced swimming speeds in a different viscous polymer solution, we analyzed their swimming speeds in viscous MC media (see Videos 3–4). In agreement with our results in PGM, we found significant differences in swimming speed distributions (Fig. 5C,D) and reduced median swimming speeds between straight rods and their respective wild-type strains (Table 2). Both straight rods mutants also showed a higher fraction of immobilized bacteria relative to their respective wild-type strains. This effect was most pronounced in PGM at 15 mg mL^{-1} where a 25 and 40% increase was observed for LSH100 and PMSS1, respectively (Table 3 and Fig. S5). Our results with straight rod mutants indicate that helical morphology enhances the fraction of motile *H. pylori* and their swimming speed. Motility enhancement was seen in all solutions but did not show an obvious dependence on viscosity.

Loss of helical morphology does not alter temporal speed variation, cell reversals, or track linearity

We utilized the cell trajectory data of the two wild-type and isogenic Δ*csd6* straight rod mutant strains to investigate whether other motility parameters were affected by perturbation of helical cell morphology. Analysis of the individual bacterium's speed standard deviations, σ_{bac}, indicated that the variation in swimming speed with time was similar for the Δ*csd6* mutants when compared to wild-type bacteria in PGM at 15 mg mL^{-1} (Fig. 5E,F) and in broth or PGM at 30 mg mL^{-1} (Fig. S6). We did not observe differences in reversal frequency between wild-type strains and their respective isogenic straight rod mutants in broth or viscous PGM or MC media (Fig. 6A,B). We also calculated the ratios of median forward swimming speed to median reversal swimming speed for individual bacterial cells that reversed and maintained at least 3 instantaneous forward or reversal speed values while swimming. We did not observe any significant differences in the ratios acquired for wild-type strains and their respective isogenic straight rod mutants in any of the solutions tested (Fig. 6C and data not shown). All strains exhibited relatively similar median ratios, close to 1 (Fig. 6C).

Finally, we examined percent track linearity (%TL) as a measure of cell path trajectory. Wild-type *H. pylori* strains showed more continuous straight runs in viscous solutions of PGM compared to broth (Fig. 7A), as previously described (Celli *et al.*, 2009). We did not observe any differences in %TL between wild-type strains and their respective isogenic straight rod mutants in broth and in viscous PGM or MC media (Fig. 7B,C, and Table S3). Thus, while wild-type *H. pylori* strains show increased %TL in their swimming trajectories in viscous solutions of PGM, this increase in % TL does not require helical cell shape. Our results indicate that while loss of helical cell shape reduces the swimming speed of *H. pylori*, helicity does not influence any other measured aspect of motility.

H. pylori swimming speed correlates with flagellum number

Our studies suggest that multiple aspects of the cell body morphology of helical bacteria may influence *H. pylori* swimming speed. In addition, flagellation may contribute to the swimming speed differences observed between wild-type *H. pylori* strains, as suggested by the increased swimming speed profiles in all media for PMSS1 which has a median flagellum number of 4 compared to 3 for B128 and LSH100 (Fig. 2F). To test the effect of flagellum number on *H. pylori* swimming speed, we utilized mutations that lead to altered flagellation in strain B128. For an isogenic strain with a reduced number of flagella, we used a *fliO*$_{\Delta C}$ mutant which bears a C-terminal truncation in the flagella export apparatus protein FliO (Tsang & Hoover, 2014) and has a median flagellum number of 1 +/− 1 (Fig. 8A). For an isogenic stain with an increased number of flagella, we used a putative small non-coding RNA mutant (designated sRNA_T; locus tag HPnc7700 in *H. pylori* 26695), which has a median flagellum number of 4 +/− 1 (Fig. 8A). sRNA_T was identified from a transcriptome analysis of *H. pylori* 26695 and is predicted to be transcribed from a FliA-dependent promoter (Sharma *et al.*, 2010). HPnc7700 is located downstream of the 16s rRNA gene and downstream of HP1439, which encodes a hypothetical protein of unknown function. HP1439 and HPnc7700 are in the same orientation and in the opposite orientation of the 16s rRNA gene. The HP1439 homolog in strain B128 (HPB128_16g92) is predicted to be longer than HP1439 (155 versus 81 amino acid residues) and overlaps the sequence coding the putative sRNA_T, and so the sRNA_T mutant is potentially deficient for both sRNA_T and the product of HPB128_16g92.

The B128 sRNA_T mutant has a flagellation profile more similar to PMSS1 (Figs 2F and 8A). In addition to perturbing flagellum number, we found that both these mutations altered other cell morphology parameters. Both the *fliO*$_{\Delta C}$ and sRNA_T mutants displayed increased cell lengths (though similar to PMSS1), and increased cell curvature profiles (but still smaller than LSH100) relative to wild-type B128 (Table S4 and Fig. S7). These results suggest that perturbation of flagella assembly may influence helical cell morphology and cell length in *H. pylori*.

We analyzed the swimming speeds of the different flagellar mutants in viscous PGM solutions (15 mg mL^{-1}) (see Videos 5–6). We were only able to analyze speeds from a small bacterial population (n=23) for the *fliO*$_{\Delta C}$ mutant because of difficulties finding fields of individual motile bacteria and because cells tended to clump (31%) as compared to wild-type (0.43%) (Table 5). A positive correlation between flagellum number and swimming

speed was observed with significantly reduced swimming speeds (50% reduction in v_m) for *fliO*$_{\Delta C}$ bacteria and increased swimming speeds (19% increase in v_m) for the sRNA_T mutant (Fig. 8B and Table 5). The B128 sRNA_T mutant also showed a higher v_m that was 18% faster than PMSS1 in this solution (14.9 μm/s vs. 12.2 μm/s) (Tables 2 and 5). The standard deviation of swimming speeds, σ_{bac}, (Fig. 8C) suggest that sRNA_T displays similar swimming dynamics to wild-type B128 (K-S, p=0.29), *fliO*$_{\Delta C}$ displays similar swimming dynamics to wild-type B128 (K-S, p=0.98), and *fliO*$_{\Delta C}$ displays similar swimming dynamics to sRNA_T (K-S, p=0.57). Thus, altering flagellation does not impact temporal behavior in the swimming speed of individual bacteria. We observed a higher fraction of immobilized bacteria (82%) for *fliO*$_{\Delta C}$, but saw a smaller fraction for the sRNA_T mutant as compared to wild-type B128 (14% vs. 36%, respectively) (Table 5).

To explore whether variation in flagellum number influences other aspects of swimming, we analyzed reversals, ratio of forward and reversal swimming speeds, and cell path trajectory for wild-type bacteria and the flagellar mutants. We observed minimal effects of changing flagellum number on reversal frequency and the ratio of forward to reverse swimming speeds (Fig. 9A,B). However, we observed differences in track linearity between wild-type and the flagellar mutants (Fig. 9C). Reduced speeds and track linearity for the *fliO*$_{\Delta C}$ mutant may result from a combination of increased cell length, increased cell curvature, and decreased flagellum number. The sRNA_T showed increased track linearity, suggesting that like PMSS1, sRNA_T may have increased directional persistence while swimming due to a higher proportion of bacteria with 4 or more flagella (Fig. 9C).

Resistive force theory modeling requires variation in both cell shape and flagellum number to explain speed differences observed between H. pylori strains

In order to gain further insight into our experimental results and the dependence of *H. pylori's* swimming speed on cell shape, we used Resistive force theory (RFT) (Gray and Hancock, 1955). RFT has previously been used to model swimming of *Caulobacter crescentus* (Li and Tang, 2006) and *Vibrio alginolyticus* (Magariyama *et al.*, 1995) by approximating their bacterial cell body as an ellipsoid and the flagellum as a rotating rigid helix. The bacteria were then assumed to swim in a Newtonian fluid and long-range hydrodynamic interactions were neglected. These simplifications make it possible to derive an analytical expression for the bacterium's swimming speed in terms of the motor torque on the flagellum, and the translational and rotational drag on the cell body and helical flagella bundle.

We used a similar approach for *H. pylori* but instead modeled its cell body as a thick helical rod, a geometry representative of its helical cell shape. The flagella bundle was modeled as a single thin helix attached at one end of the helical cell body. With this geometry, the equations of motion for the cell body and flagellum can be written and solved analytically (for details on this derivation see Experimental Procedures). The final result is that swimming speed is proportional to the flagella bundle motor torque, T_m, via a shape factor S_h, $v_h = S_h T_m$. The motor torque, T_m, represents the influence of the flagella motors on swimming while the shape factor, S_h, represents the effects of the translational and rotational drag of the cell body and flagella bundle. The shape factor relies on cell body and flagella

geometry, and although the motor torque for *H. pylori* has yet to be measured, analysis of the shape factor provides insight into how different cell geometries affect swimming speed, with some geometries more efficiently converting motor torque to speed.

To examine how the shape factor depends on cell body helical parameters, we calculated S_h for a typical *H. pylori* bacterium with a cell length $L = 3.1$ μm, helical pitch $P = 2.5$ μm, helical radius $R = 0.15$ μm, and cell diameter $D = 0.56$ μm. These cell body parameters are the mean cell body measurements acquired for the three wild-type *H. pylori* strains: LSH100, B128, and PMSS1 (Table 1). For the flagella bundle, we used a bundle thickness of $d = 0.07$ μm; a flagellum pitch of $p = 1.58$ μm; and a helical radius of $r = 0.14$ μm (see Experimental Procedures); and a flagellum length of $l = 4.1$ μm (the mean flagellum length of all the wild-type strains). Figure 10 shows the dependence of S_h on one cell shape parameter at a time (L, P, or R) keeping the other two parameters constant. In the parameter ranges observed for *H. pylori* (shaded blue region), S_h decreases monotonically with increasing L or R (Fig. 10A,B), while it exhibits a non-monotonic dependence on P (Fig. 10C), exhibiting a shallow maximum at $P \approx 3.4$ μm with a very slight decrease thereafter. This maximum corresponds to a speed maximum for bacteria with a pitch angle of approximately 15º. Our model predicts that in order to have a large S_h value, and hence a faster speed for the same motor torque, a helical cell must have a short cell length, small helical radius, and a helical pitch of approximately 3.4 μm.

To compare how the variation in cell shape for the different strains alters their shape factor, we calculated S_h for LSH100, B128, PMSS1, and the B128 sRNA_T flagellar mutant (Table 6). For each strain, S_h was calculated using their average cell body parameters (Table 1 and Table S3) and the same flagella bundle parameters described above. Table 6 shows that S_h for LSH100, PMSS1, and B128 sRNA_T all have similar values, while B128 has the largest S_h value (10% larger than all other strains). This is a result of the small average cell length and helical radius of B128 as compared to the other strains (Table 1). These shape factor differences would produce about a 10% change in swimming speed if all strains produced a similar motor torque on the flagella bundle. However, the differences in swimming speed in PGM at 15 mg mL^{-1} were observed to be much larger (~ 0 – 90%). By comparing the ratios of shape factors to the ratios of swimming speeds (Table 6), we conclude that differences in shape factor alone do not fully explain the differences observed between wild-type strains in their experimental swimming speeds.

Our experimental results show that *H. pylori* strains vary flagellum number (Fig. 2F) and flagellum number correlates with swimming speed (Fig. 8). Based on this, we make the simplest hypothesis that the flagella bundle motor torque, T_m, increases proportionally with the number of flagella (N_f) in the flagella bundle, where $T_m = N_f T_f$ and T_f is the torque produced by a single flagellum. With this modification the swimming speed can be written as a function of both the shape factor and flagellum number, $v_h = (S_h N_f) T_f$. Table 6 shows the product of $S_h N_f$ as calculated for each wild-type strain and the sRNA_T mutant using their respective median flagellum numbers. The product of the shape factor and flagellum number predicts larger differences, ~20–30% among the different strains as compared to the shape factors alone. The ratio of $S_h N_f$ agrees very well with the experimental ratio of swimming speeds observed for B128 and its flagellar mutant sRNA_T, thus, reflecting

primarily the change in flagellum number, albeit with a small variation in cell length. The predicted ratio of $S_h N_f$ for B128 and sRNA_T, relative to PMSS1, were within 10% of their measured speed ratios (Table 6). However, for LSH100 compared to PMSS1, the predicted ratio of $S_h N_f$ does not agree well with the experimentally measured ratio of speeds, suggesting that the RFT model has some limitations in modeling the effects of helical shape.

Discussion

While variation in cell morphologic parameters among strains and between species have long been noted, our studies provide an in-depth, quantitative analysis of *H. pylori's* natural variation in helical cell and flagellum morphology, and how these parameters impact *H. pylori's* motility in viscous environments. Most of the previous studies of *H. pylori* motility provide numbers for only the average or maximum speed. Given the wide distribution of speeds, we suggest that conclusions based only on the variation of a single speed parameter with varying external conditions could be misleading as the shape of these broad, asymmetric distributions is not fully described by a single parameter such as the average, thus higher moments of the distribution are required to describe the shape of an asymmetric distribution. Our motility studies of three unrelated wild-type *H. pylori* strains in broth and viscous solutions of PGM reveal the swimming speed distributions reflect both temporal variation in the speed of individual bacteria (Fig. 4) and morphological variation within the population (Fig. 2).

The observed broad distribution of swimming speeds was largely due to temporal variation in swimming speed, which we characterized using the distribution of individual bacterium's standard deviation in speed, σ_{bac} (Fig. 4). Wild-type *H. pylori* strains exhibited temporal variation that was dependent on their swimming environment, however loss of helical cell shape or perturbed flagellation did not affect how individual bacteria vary their swimming speed with time. Our data suggest that temporal speed variation is not influenced by morphology, but can be influenced by bacteria-medium interactions, and may reflect fluctuations due to flagella bundling-unbundling events and/or the stochastic behavior in motor activity.

The speed distributions also vary depending on which polymer solution (and at what concentration) the bacteria swims in. Of particular interest is the observation that compared to broth *H. pylori's* swimming speeds are slightly higher in PGM at both physiologically relevant concentrations; the higher mucin concentration corresponding to that in the mucus close to the epithelial surface, and the lower mucin concentration similar to that in the luminal layer. We observed a non-monotonic variation in *H. pylori* swimming speed, and increased proportions of immobile bacteria as the viscosity of PGM increased (Table 3 and Fig. S5). Caldara *et al.* observed a similar behavior in *Pseudomonas aeruginosa*, where bacteria displayed increased swimming speeds in PGM (although at lower PGM concentrations) (Caldara *et al.*, 2012). Yeung *et al.* found that addition of mucin at physiological concentrations promoted the ability of *P. aeruginosa* to exhibit rapid motility across the surface of agar (Yeung *et al.*, 2012). The physical mechanism responsible for the increase in motility of *H. pylori* in viscous PGM solutions is unclear. Possible factors may relate to molecular interactions of bacteria with mucin and the viscoelastic nature of mucin

solutions. Recent studies suggest *H. pylori* may directly bind mucins and glycolipids in gastric mucus (Naughton *et al.*, 2013), and there is a growing body of theoretical work exploring how polymer viscoelasticity alters bacterial swimming (Lauga and Powers, 2009).

In methylcellulose, we observed an increase in swimming speed, at a viscosity of 26 cP, followed by a decrease at a higher viscosity of 76 cP (Table 2). This non-monotonic behavior agrees with previous *H. pylori* motility studies in methylcellulose (Worku *et al.*, 1999), along with other studies of bacteria in viscous polymer solutions (Shoesmith, 1960; Schneider and Doetsch, 1974; Greenberg and Canale-Parola, 1977a; Ferrero and Lee, 1988). Recent work by Martinez *et al.* suggests that this non-monotonic behavior may be caused by non-Newtonian shear thinning causing the flagellum to experience a lower effective viscosity than the cell body (Martinez *et al.*, 2014). We did not probe the length and time scales at which flagella interact with the polymer environment in this study and leave quantifying the shear thinning effects of gastric mucin and methylcellulose on bacterial motility for future work.

To directly address the impact of *H. pylori's* helical cell body shape on motility, we examined the swimming speeds of isogenic straight rod mutants that had similar flagellum length and number to wild-type bacteria. In PGM solutions, which best mimic the different rheological environments *H. pylori* experiences in the stomach, we observed an 8–13% increase in speed of the helical bacteria compared to straight rods (Table 2). We also observed that helical cell shape increased the fraction of motile bacteria (Fig. S5 and Table 3). This effect was most pronounced in PGM concentrations that resemble the mucin concentrations found in the outer mucus layer, which *H. pylori* must quickly penetrate to escape from the acidic lumen.

The effect of helical shape on motility has been explored in Spirochete bacteria that have periplasmic flagella and utilize a running wave mode of translational motility distinct from that used by bacteria with external flagella (Dombrowski *et al.*, 2009; Charon *et al.*, 2012). Spontaneous mutants of *Spirochaeta halophila* that retain flagella but have lost helical cell morphology show decreases in maximal swimming velocity and a lower minimum immobilizing viscosity (MIV) (Greenberg and Canale-Parola, 1977b). Interestingly, this study also explored the behavior of related strains and species that varied in their helical parameters, characterized as having “tight” or “loose” coils. While they did not observe a correlation between helical pitch and maximum velocity or the viscosity at which maximum velocity occurred, they observed marked variation in the MIV (300–1,000 cP) among strains with “tight” coils having the highest MIV. While helical parameters were not precisely quantified, their results appear consistent with our observations that helical shape provided a similar increase in swimming speed regardless of viscosity of the medium or helical pitch angle of the parent strain, as well as a more pronounced effect of helical morphology on the percent of immobile bacteria.

Recently Liu *et al.* observed that *Caulobacter crescentus*, a bacteria with crescent cell shape and external flagella, enhances its motility by precessing its crescent cell body in a helical trajectory (Liu *et al.*, 2014). Although these bacteria have a different cell geometry compared to *H. pylori*, their findings are consistent with our observations that the shape of

the cell body can enhance flagella-mediated motility. Overall, our findings on the effect of *H. pylori's* helical cell shape on its motility add to a growing consensus that the bacterial cell bodies may play a larger role in motility than previously thought.

In addition to cell shape, we also measured a significant contribution of flagellum number to *H. pylori* swimming speed. Increased flagellation (+1) of B128 through deletion of the sRNA_T gene resulted in an increase in median swimming speed (19%), track linearity, and a smaller fraction of bacteria immobilized in PGM (Figs 8 and 9, and Table 5). The sRNA_T mutant bacteria were also longer than the parent strain B128 (Table S3), suggesting that an increase in flagellum number may enhance flagellar propulsion and overcome the propulsive drag provided by helical bacteria with increased cell length. Work by Mears *et al.* found an analogous finding for *E. coli*, as cells with increased flagellum number were observed to have increased cell length and a slight increase in swimming speed (Mears, 2014). In another *E.coli* study, Darnton *et al.* suggested that torque on a single flagellum and the flagella bundle are similar and an increase in flagellum number does not result in an increase in swimming speed (Darnton *et al.*, 2007). They postulated that torque is dissipated when the peritrichous flagella of *E. coli* have to bend around the cell body to form the flagella bundle (Darnton *et al.*, 2007). Perhaps consistent with this finding, induction of secondary lateral flagella in the single polar flagellated bacterium *Shewanella putrefaciens* resulted in higher directional persistence and spreading in soft agar, but lower swimming speeds (Bubendorfer *et al.*, 2014). The lophotrichous flagella of *H. pylori* may lessen this effect, but as of now its flagella bundling behavior has not been explored. Future experiments imaging the flagella of swimming bacteria should shine light on the flagella bundling behavior and the effect altering flagellum number has on bundling.

To further understand the role of cell morphology on swimming speed, we compared the influence of helical cell shape and number of flagella on swimming speed using a resistive force theory model. Assuming a constant motor torque, the swimming speed of a helical bacteria is predicted to decrease with increasing cell length and helical radius, suggesting the fastest swimming speeds are obtained by bacteria with small cell lengths and small radii. However, altering helical cell shape led to a relatively small change in the RFT predicted swimming speeds, ~ 10%, in contrast to the large changes in swimming speeds observed experimentally (as much as a 90%) for wild-type strains with different shape morphologies. Varying the motor torque using a simple linear dependence of motor torque on flagellum number produced a larger change in swimming speed, 20–30%, than that produced by only altering cell shape. Combining both the effect of cell shape and flagellum number, we were able to explain the observed differences in swimming speed for B128 and its flagellar mutant, which reflect mostly the change in flagellum number. Comparing the other strains, which differ in both flagellum number and shape, produced mixed results. A comparison of the ratios of RFT predictions for PMSS1 to those of B128 and sRNA_T showed better agreement with experimental results than predictions comparing PMSS1 to LSH100. Our results indicate that while both cell shape and flagellum number independently affect swimming speed, flagellum number contributes to a larger alteration in speed as compared to changing cell shape. Recent modeling studies of bacteria with different numbers of peritrichous flagella predict that swimming speed increases logarithmically with increased flagellation (Kanehl and Ishikawa, 2014). While we assumed a linear model based on our

experimental observations, a logarithmic dependence gives comparable results, predicting an increase of ~ 26% when comparing bacteria with four vs. three flagella, and supports our observations that swimming speed correlates with flagellum number.

While the RFT model provided insight into the relative effect of cell shape and flagellum number on swimming speed it has inherent limitations. In particular, the model predictions are based on cell shape parameters of an average or "typical" bacterium. However, the average or median speed measured from the speed distribution does not correspond to the speed of the average bacterium. Hence, the present state of modeling is capable of qualitative predictions, and one has to be careful in drawing detailed quantitative comparisons. The model's underestimation of the speed difference between LSH100 and PMSS1 also suggests it may underestimate the shape factor due to the more curved shape of LSH100. Recent work by Rodenborn *et al.* showed that RFT can lead to inaccurate predictions for a helical flagellum with helical parameters in the range of $L>3P$ or $P<6R$ (Rodenborn *et al.*, 2013). These inaccuracies are due to RFT neglecting long-range interactions of the fluid flow from different parts of the helix. While our calculations for the cell body are outside the cited ranges, $L/P \approx 1.2$ and $P/R \approx 10$, Rodenborn *et al.* modeled a very thin helix (helical thickness to helical radius $D/R \approx 0.06$), which was meant to mimic the flagellum. For the *H. pylori* cell body, the helical radius is comparable to the cell thickness $D/R \approx 2$, meaning long-range hydrodynamic interactions may play a larger role. In light of this, we are currently exploring the use of a numerical solution of the hydrodynamic equations based on a regularized Stokeslet method (Cortez *et al.*, 2005) to further probe the swimming of helical cells.

Another aspect absent in our model is medium specific interactions. Our experimental results show medium specific changes in *H. pylori* swimming speed and temporal swimming behavior, which the RFT model cannot explain. Recently, Spagnolie *et al.* modeled a rotating helix in a viscoelastic fluid and showed that the swimming speed of the helix can increase or decrease depending on the combination of its helical parameters and the viscoelastic parameters of the medium (Spagnolie *et al.*, 2013). These effects could explain the increase in swimming speeds we observed for helical bacteria swimming in PGM solutions, however making any direct link between swimming speed and swimming medium properties requires further study.

While efficient motility is essential for persistent colonization of the gastric mucus layer by this pathogen to get to its extracellular niche and during turnover of mucus and gastric epithelial cells, our study raises the question as to whether there may be selective pressures in addition to swimming speed that dictate *H. pylori* cell shape and flagellum number. Although both helicity and flagellum number alter swimming speed, it is noteworthy that their alteration resulted in a smaller change in speed (~1 μm/s) than the observed changes in an individual bacterium's speed with time (~1–5 μm/s). In addition, growth of a subpopulation of straight rod and curved cells along with bacteria with zero to two flagella persist in all strains analyzed (this work and Sycuro *et al.*, 2010). Having cells within the population with less flagella or a straight rod shape may play an unknown benefit to *H. pylori* unrelated to motility. Extending our cell-based morphologic studies to infected

stomach tissues may begin to reveal whether different morphologies favor different niches within the stomach that include the surface mucus, gastric glands, and epithelial cell surface.

Experimental Procedures

Bacterial strains and culture conditions

Strains used in this study are described in Table S1. We used three unrelated wild-type *H. pylori* strains: LSH100, a derivative of the sequenced human clinical isolate G27 (Baltrus *et al.*, 2009; Lowenthal *et al.*, 2009); PMSS1, also called 10700 (Lee *et al.*, 1997; Arnold *et al.*, 2011); and B128 (McClain *et al.*, 2009) and mutant derivatives of these strains. Bacteria were cultured on horse blood plates or in liquid media containing 90% (v/v) Brucella broth (BD Biosciences) and 10% fetal bovine serum (GIBCO) (BB10) in the absence of antimicrobials as previously described (Sycuro *et al.*, 2010). Cells were maintained at 37ºC under microaerobic conditions in a tri-gas incubator equilibrated to 10% CO_2 and 10% O_2. Plates were incubated 24–72 hours and liquid cultures were incubated for 12–16 hours under constant agitation at 200 rpm. For resistance marker selection, horse blood plates were supplemented with chloramphenicol (15 μg mL^{-1}).

Morphology analysis

Wild-type *H. pylori* LSH100 and PMSS1, and wild-type B128 and its respective flagellar mutants (*fliO*$_{\Delta C}$ and sRNA_T) were grown in liquid culture to an optical density at 600 nm (O.D. $_{(600)}$) of 0.3–0.7. Bacteria were fixed (4% Paraformaldehyde, 1X PBS, and 25% Glycerol) and added to 0.1% poly-L-lysine (Sigma Aldrich) coated coverslips that were placed on a pre-cleaned microscope slide, and were then sealed with VaLP (1:1:1 Vaseline: Lanolin: Paraffin). Single focal plane images were collected using a 100 X ELWD Plan APO (NA 1.40 oil) objective mounted on a Nikon TE 200 microscope, equipped with a Nikon CoolSNAP HQ CCD camera controlled by MetaMorph software (MDS Analytical Technologies). Quantitative morphology analysis of manually thresholded phase-contrast images was performed as described in Sycuro *et al.* using the CellTool software program (Lacayo *et al.*, 2007; Pincus & Theriot, 2007; Sycuro *et al.*, 2010). Centerline data for each strain was obtained from CellTool, imported to MATLAB, and fitted to a generalized sine curve, $y=R\sin(\frac{2\pi}{P}x+\delta)$, where R and P represent the helical radius and helical pitch, respectively, and δ is a phase term added to allow for an arbitrary origin of the sine function. Cells with non-helical morphologies resulted in poor fitting, characterized by a large sum of squared error (SSE > 0.2), and were removed from our data sets. The number of cells used to generate cell shape models were LSH100, n=262; PMSS1, n=215; B128; n=272; B128 *fliO*$_{\Delta C}$, n=296; and B128 sRNA_T, n=305.

Transmission Electron Microscopy (TEM) and Scanning Electron Microscopy (SEM) of H. pylori cells

TEM of *H. pylori* was performed as described in Lowenthal *et al.*, 2009, and cells were visualized with a JEOL JEM 1400 transmission electron microscope. SEM of *H. pylori* was performed as described in Sycuro *et al.*, 2013. Digital images were manipulated using Image J and Adobe Photoshop.

H. pylori flagellum length measurements and flagellum number counts

Flagellum number counts were acquired from SEM (LSH100 and PMSS1 and their respective straight rod mutants) or TEM images (B128 and the flagellar mutants). The number of flagella was counted from 83 – 110 different bacteria per strain. Flagellum length measurements were acquired from TEM images collected from the same preparation for all strains. TEM images were uploaded to Image J and calibrated using the scale bar (1 μm) of images acquired at 2500 – 3000 X. Using the segmented line selection tool, flagellum length was measured for one flagellum per cell, four times each, from 15 different bacteria per strain to provide average lengths and standard deviations from the means.

Generation of knockout isogenic mutants

An isogenic mutant of *csd6* (HPG27_477) in the PMSS1 strain background was generated by transfer of the mutation constructed in the LSH100 strain background (Sycuro *et al.*, 2013) using natural transformation (Wang *et al.*, 1993). Transformants were confirmed by PCR using primers homologous to upstream and downstream flanking regions for each gene using the primers indicated in Table S2. The mutation was then backcrossed into PMSS1 once by isolating genomic DNA from the resulting strain for natural transformation of PMSS1. The resulting backcrossed clones were evaluated by PCR to confirm replacement of the wild-type allele with the null allele (*csd6*). Clones were checked for urease activity and motility, and single clones were used for quantitative morphology analyses and the motility studies.

An isogenic mutant of *motB* (HPG27_772) was constructed in the LSH100 strain background as described above. Genomic DNA of *motB* bearing a transposon insertion was acquired from the mutant library generated in *H. pylori* G27 (Salama *et al.*, 2004) and was used for natural transformation of LSH100.

Deletion of sRNA_T was generated in *H. pylori* B128 by the following procedure. Overlapping PCR was used to generate an amplicon that contained a kanamycin resistance cassette (*aphA3*) gene flanked by ~500 bp regions located upstream and downstream of the target sRNA. Primers used for PCR are listed in Table S2. The region upstream of sRNA_T was amplified using the upstream forward and the upstream reverse primers. The 5′-end of the upstream reverse primer contained sequence corresponding to one end of the *aphA3* cassette. The region downstream of sRNA_T was amplified using the downstream forward and the downstream reverse primers. The 5′-end of the downstream forward primer contained sequence corresponding to the other end of the *aphA3* cassette. The *aphA3* cassette was amplified using the kan forward and kan reverse primers. Overlapping PCR via the complementary regions of the amplified *aphA3* cassette and the amplicons of the regions flanking the target gene generated a PCR product with the *aphA3* cassette between the flanking regions. The resulting amplicon was introduced into *H. pylori* B128 by natural transformation. Replacement of sRNA_T with the *aphA3* cassette was confirmed by PCR using genomic DNA from kanamycin resistant transformants as a template, and was further verified by sequencing the resulting amplicons.

Preparation of purified PGM

PGM was isolated from mucosal scrapings of pig stomach epithelium and purified by Sepharose CL-2B column chromatography followed by density gradient ultracentrifugation as described in (Celli *et al.*, 2009). Lyophilized PGM powder was allowed to reach room temperature before opening tubes to avoid condensation. The powder was weighed and 7.5 mg was dissolved in 400 μL of sterile H_2O to prepare a 15 mg mL^{-1} solution with bacteria, and 15 mg was dissolved in 800 μL of sterile H_2O to prepare a 30 mg mL^{-1} solution with bacteria. PGM was allowed to hydrate and equilibrate for 48 hours at 4ºC before use.

Preparation of methylcellulose

Stock solutions of methylcellulose (MC) from Sigma Aldrich (M0261) were prepared by making 20 mg mL^{-1} (wt/vol) solutions in sterile H_2O, where the mixture was slowly agitated overnight at room temperature using a tube rotator. The approximate viscosity of a 20 mg mL^{-1} MC solution was 400 cP (approximate molecular weight, 41,000, Sigma Aldrich, M 0262).

Measuring the viscosity of broth and viscous media by particle-tracking microrheology

Fluorescent polystyrene latex beads (1.001 +/− 0.01 μm diameter) (Polysciences Inc.) were added to broth or viscous PGM or MC sample to provide a final bead concentration of 0.05% beads by volume in a final volume of 1 mL. Flagellated but nonmotile bacteria (LSH100 Δ*motB*) were grown in liquid broth (BB10) at an $O.D._{(600)}$ of 0.3 – 0.7. Bacteria was added to each solution to produce a 10% bacteria mixture by volume, and bacteria were examined after 45 min of incubation in each solution at 37ºC under microaerobic conditions. A 10 μL volume of bead or bacteria solution was then pipetted onto a glass slide with a secure spacer (Secure-Seal, Sigma-Aldrich) and covered with a coverslip. Samples were imaged using an Olympus IX 70 microscope (40 X Plan N, 0.45 NA) with QCAM CCD camera (Qimaging) at 20 fps and 0.2312 μm pixel size. Fluorescent beads were excited using an Olympus BH2 Mercury arc source while bacteria were imaged using phase contrast with light from a halogen bulb. Focus was set to the center and middle Z-positions of the sample in order to minimize edge effects. Videos were captured at 30 s intervals using Micro-Manager open source acquisition software (Edelstein *et al.*, 2010) and were analyzed in MATLAB v7.12.0 using a particle-tracking routine that finds the center of intensity of each bead or bacterium using a polynomial Gaussian fit (Rogers *et al.*, 2007). Beads or bacterium that drifted were dedrifted using a custom MATLAB routine and superfluous tracked objects were removed.

Motility assay in purified PGM and methylcellulose solutions

Bacteria were grown in liquid culture broth to an $O.D._{(600)}$ of 0.5 – 0.7 and kept warm at 37°C under microaerobic conditions until use. 10 μL of culture was added to 80 μL of PGM solution and 10 μL of pH 6 buffer (0.1 M phosphate-succinate) to produce a 10% bacteria mixture by volume and the final PGM concentrations used were 15 mg mL^{-1} and 30 mg mL^{-1}. For methylcellulose solutions, 10 μL of culture was added to a solution that consisted of 50 μL of MC stock solution (20 mg mL^{-1}) and 40 μL of pH 6 buffer (0.1 M phosphate-succinate), to produce a 10% bacteria mixture by volume and a final concentration of MC at

10 mg mL^{-1}. To produce a 10% bacteria mixture by volume and a final concentration of MC at 15 mg mL^{-1}, 10 μL of culture was added to 75 μL of MC solution (20 mg mL^{-1}) and 15 μL of pH 6 buffer (0.1 M phosphate-succinate). Bacteria were incubated for 45 min in their respective PGM or MC solutions at 37ºC under microaerobic conditions prior to imaging. After the incubation period, each cell suspension was mixed by gentle pipetting and 10 μL was applied to standard glass microscope slides with secure imaging spacers (9 mm in diameter × 0.12 mm depth, Secure-Seal, Sigma-Aldrich). A coverslip was placed over the sample and was securely sealed. Samples were immediately imaged at room temperature using a Nikon TE 200 inverted microscope (60 X ELWD Plan Fluor, 0.7 NA Phase lens, depth field of ~5 μm) and ten second videos were captured for bacteria swimming in the mid-level plane between the coverslip and glass slide, which is ~60 μm in depth, using a Nikon CoolSNAP HQ CCD camera (100 millisecond intervals over a 10 s period (10 fps), 0.109 μm/pixel) and MetaMorph software (MDS Analytical Technologies). Bacteria were tracked using the Volocity software (v6.1) (Elmer, 2011).

Tracking of swimming bacteria using Volocity (v6.1)

Videos were processed and converted to 8-bit files using ImageJ (Rasband, 1997–2014) and uploaded to the particle-tracking program in Volocity v6.1 to generate tracks based on the centroid position of each object identified (area, 0.05 – 8.0 μm^2). Individual trajectories were obtained for at least 10 frames of the video (1 s) (see Fig. S1). Bacteria showing a displacement less than 0.3 μm or a mean squared displacement (MSD) less than 0.1 μm^2 were considered to be immobile and were removed. Individual trajectories of 100 bacteria were acquired, examined visually to ensure accuracy, and imported into MATLAB v7.12.0 for smoothing using a five point Savitsky-Golay filter to remove noise effects caused by wiggling trajectories (Hyon *et al.*, 2012) and finite tracking resolution (Son *et al.*, 2013). Stops, reorientations, swimming speeds, and reversal events were segmented and were used to describe *H. pylori* motion.

Analysis of the fraction of immobile bacteria in broth and viscous PGM media

Videos gathered for tracking individual bacterial cells for velocity analysis were used to determine the fraction of motile and nonmotile (immobilized) bacteria in broth and PGM media. We classified all bacteria with displacements less than 0.3 μm as immobile and bacteria with displacements greater than 0.3 μm as motile. The percentage of immobilized bacteria was calculated by dividing the total number of nonmotile cells by the total number of bacterial cells. The total bacterial population included nonmotile bacteria and motile bacteria (bacteria with displacements between 0.3 – 1.5 μm, and bacteria with displacements > 1.5 μm that were processed through MATLAB and segmented to acquire swimming speeds after tracking by Volocity). The number of clumped bacteria (clusters of aggregated bacteria) was analyzed for B128 and the flagellar mutants in viscous PGM solutions (15 mg mL^{-1}). The percentage of clumped bacteria was calculated by dividing the total number of clumps by the total bacterial population. The total bacterial population consisted of the number of clumped bacteria, nonmotile cells (individual cells with displacements < 0.3 μm), and motile cells (as described above).

Resistive force theory mathematical modeling

At low Reynolds number the forces, F_c and F_f, and torques, T_c and T_f, on a bacterium must balance.

$$F_c+F_f=0$$
$$T_c-T_f=0$$
$$T_m-T_f=0$$

Here *c, f*, and *m* denote the cell body, flagellum, and motor, respectively. Resistive force theory states that the forces and torques on an object are proportional to the local speed and angular rotation rate of that object, with the constant of proportionality determined by the object's geometry and viscosity of the liquid (Gray and Hancock, 1955).

We modeled the cell body of wild-type *H. pylori* as a rigid helix while the bacterium's helical flagellum was assumed to bundle and form a single helix. The total force on a translating and rotating helix is a sum of the translational drag, $F_{drag} = -\alpha_h v_h$, and rotational propulsion, $F_{propulsion} = \gamma_h \omega_h$, while total torque is a sum of the rotation drag, $T_{drag} = \beta_h \omega_h$, and translation drag, $T_{propulsion} = -\gamma_h v_h$. Here α_h, β_h, and γ_h represent the translational, rotational, and propulsion drag coefficients of a helical cell body, respectively. In an analogous way, the flagellum has translational, rotational, and propulsion drag coefficients which we designate as α_f, β_f, and γ_f.

Using the force and torque equations above, along with force torque balance between the cell body and flagellum, we solved for the swimming speed of a helical cell body, v_h, in terms of the motor torque, T_m. The swimming speed can be written as the product of T_m, and a shape factor, S_h, that depends on the cell body and flagellum drag coefficients.

$$v_h = S_h T_m$$
$$S_h = \frac{\frac{\gamma_h}{\beta_h}+\frac{\gamma_f}{\beta_f}}{\alpha_h+\alpha_f-\frac{\gamma_h}{\beta_h}\gamma_h-\frac{\gamma_f}{\beta_f}\gamma_f}$$

To calculate S_h we used previously derived expressions for α_h, β_h, and γ_h in terms of the cell body parameters: cell length (L), helical pitch (P), helical radius (R), and pitch angle (Φ) (Rodenborn *et al.*, 2013) with local normal (C_n) and tangential (C_t) force expressions derived by Gray and Hancock (Gray and Hancock, 1955). Using the same formula, the flagellum coefficients α_f, β_f, and γ_f, can be written in terms of the flagellum helical length (l), pitch (p), radius (r), pitch angle (φ), and local normal (c_n) and tangential (c_t) forces.

$$\alpha_h = (C_n \sin^2(\Phi) + C_t \cos^2(\Phi))L$$
$$\beta_h = (C_n \cos^2(\Phi) + C_t \sin^2(\Phi))R^2 L$$
$$\gamma_h = (C_n - C_t)\sin(\Phi)\cos(\Phi)RL$$
$$\alpha_f = (c_n \sin^2(\phi) + c_t \cos^2(\phi))l$$
$$\beta_f = (c_n \cos^2(\phi) + c_t \sin^2(\phi))r^2 l$$
$$\gamma_f = (c_n - c_t)\sin(\phi)\cos(\phi)rl$$

Using these expressions, the drag coefficients and shape factor were calculated using average cell shape measurements acquired from CellTool (Fig. 2). For wild-type *H. pylori* strains, we used the average helical parameters acquired from fitting the centerlines of each bacterial cell within each wild-type population (Fig. 2B and Table 1). We acquired a uniform flagellum diameter (*d,* ~0.07 μm), and used the average flagellum length (*l*) acquired from measurements done on TEM and SEM images (Fig. 2 and Table 4, and Fig. S3). Because the flagellum helical pitch (*p*) and helical radius (*r*) for *H. pylori* have not been measured, we assumed a helical flagellum form similar to that of *Vibrio alginolyticus*, where $p = 1.58$ μm and $r = 0.14$ μm (Magariyama *et al.*, 1995) for all bacteria examined in this study. All numerical calculations and manipulations were done using MATLAB v7.12.

Statistical analysis

We used the Kolmogorov-Smirnov (K-S) statistics tool in CellTool to assay differences in cell shape morphology, including cell length and side curvature distributions, as described in detail in Sycuro *et al.*, 2010 and 2012. To make statistical comparisons between wild-type helical radius, helical pitch, and pitch angle distributions, and comparisons between wild-type vs. mutant temporal variation in swimming speed, unpaired nonparametric Kolmogorov-Smirnov (K-S) tests were performed using MATLAB v7.12.0. To make statistical comparisons between wild-type vs. mutant instantaneous speed distributions; cell path trajectories; frequency of reversals; and the ratios of forward and reversal swimming speeds; unpaired nonparametric Kolmogorov-Smirnov (K-S) tests were performed using GraphPad Prism version 6.00 for Windows (GraphPad Software, La Jolla, CA USA). Statistics for the temporal analysis of wild-type vs. mutant was done using unpaired nonparametric Kolmogorov-Smirnov (K-S) tests in MATLAB v7.12.0. For each comparison, a K-S p-value < 0.05 was considered significant.

Supplementary Material

Refer to Web version on PubMed Central for supplementary material.

Acknowledgments

This work was supported by US National Institute of Health Grants R01 AI094834 (N.R.S.), F31 AI098424 (L.E.M.), R25 CA153955 (J.M.H.), R00 AG042487 (Z.P.), and the National Science Foundation PHY 1058648 and PHY 1410798 (R.B.), MCB-1244242 (T.R.H.). The funders have no role in study design, data collection and interpretation, or the decision to submit the work for publication. The contents are solely the responsibilities of the authors and do not necessarily represent the official views of these funding agencies. We thank Prof. Jonathan P. Celli for helpful discussions regarding his work on *H. pylori* motility in PGM; Dr. Bradley Turner for very helpful discussions regarding mucin and providing purified porcine gastric mucin; Dave McDonald and Julio Vasquez (FHCRC Scientific Imaging Core) for help with bacterial tracking analysis; Sharmon Knecht, Bobbie Schneider, and Stephen MacFarlane (FHCRC Electron Microscopy Shared Resource) for assistance with TEM and SEM.

References

Arnold IC, Lee JY, Amieva MR, Roers A, Flavell RA, Sparwasser T, Müller A. Tolerance rather than immunity protects from *Helicobacter pylori*-induced gastric preneoplasia. Gastroenterology. 2011; 140:199–209. [PubMed: 20600031]

Asakura H, Churin Y, Bauer B, Boettcher JP, Bartfeld S, Hashii N, et al. *Helicobacter pylori* HP0518 affects flagellin glycosylation to alter bacterial motility. Mol Microbiol. 2010; 78:1130–1144. [PubMed: 21091500]

Baltrus DA, Amieva MR, Covacci A, Lowe TM, Merrell DS, Ottemann KM, et al. The complete genome sequence of *Helicobacter pylori* strain G27. J Bacteriol. 2009; 191:447–448. [PubMed: 18952803]

Bansil R, Celli JP, Hardcastle JM, Turner BS. The Influence of Mucus Microstructure and Rheology in *Helicobacter pylori* Infection. Front Immunol. 2013; 4:310. [PubMed: 24133493]

Bell AE, Allen A, Morris ER, Ross-Murphy SB. Functional interactions of gastric mucus glycoprotein. Int J Biol Macromolec. 1984; 6:309–325.

Bell AE, Sellers LA, Allen A, Cunliffe WJ, Morris ER, Ross-Murphy SB. Properties of gastric and duodenal mucus: effect of proteolysis, disulfide reduction, bile, acid, ethanol, and hypertonicity on mucus gel structure. Gastroenterology. 1985; 88:269–280. [PubMed: 3917263]

Berg HC, Turner L. Movement of microorganisms in viscous environments. Nature. 1979; 278:349–351. [PubMed: 370610]

Bonis M, Ecobichon C, Guadagnini S, Prevost MC, Boneca IG. A M23B family metallopeptidase of *Helicobacter pylori* required for cell shape, pole formation and virulence. Mol Microbiol. 2010; 78:809–819. [PubMed: 20815828]

Bubendorfer S, Koltai M, Rossmann F, Sourjik V, Thormann KM. Secondary bacterial flagellar system improves bacterial spreading by increasing the directional persistence of swimming. Proc Natl Acad Sci U S A. 2014; 111:11485–11490. [PubMed: 25049414]

Cabeen MT, Jacobs-Wagner C. Bacterial cell shape. Nat Rev Microbiol. 2005; 3:601–610. [PubMed: 16012516]

Caldara M, Friedlander RS, Kavanaugh NL, Aizenberg J, Foster KR, Ribbeck K. Mucin biopolymers prevent bacterial aggregation by retaining cells in the free-swimming state. Curr Biol. 2012; 22:2325–2330. [PubMed: 23142047]

Celli J, Gregor B, Turner B, Afdhal NH, Bansil R, Erramilli S. Viscoelastic properties and dynamics of porcine gastric mucin. Biomacromolecules. 2005; 6:1329–1333. [PubMed: 15877349]

Celli JP, Turner BS, Afdhal NH, Ewoldt RH, McKinley GH, Bansil R, Erramilli S. Rheology of gastric mucin exhibits a pH-dependent sol-gel transition. Biomacromolecules. 2007; 8:1580–1586. [PubMed: 17402780]

Celli JP, Turner BS, Afdhal NH, Keates S, Ghiran I, Kelly CP, et al. *Helicobacter pylori* moves through mucus by reducing mucin viscoelasticity. Proc Natl Acad Sci U S A. 2009; 106:14321–14326. [PubMed: 19706518]

Charon NW, Cockburn A, Li C, Liu J, Miller KA, Miller MR, Motaleb MA, Wolgemuth CW. The unique paradigm of spirochete motility and chemotaxis. Annu Rev Microbiol. 2012; 66:349–370. [PubMed: 22994496]

Cicuta P, Donald AM. Microrheology: a review of the method and applications. Soft Matter. 2007; 3:1449.

Cortez R, Fauci L, Medovikov A. The method of regularized Stokeslets in three dimensions: Analysis, validation, and application to helical swimming. Physics of Fluids. 2005; 17:031504.

Darnton NC, Turner L, Rojevsky S, Berg HC. On torque and tumbling in swimming *Escherichia coli*. J Bacteriol. 2007; 189:1756–1764. [PubMed: 17189361]

Dombrowski C, Kan W, Motaleb MA, Charon NW, Goldstein RE, Wolgemuth CW. The elastic basis for the shape of Borrelia burgdorferi. Biophys J. 2009; 96:4409–4417. [PubMed: 19486665]

Duan Q, Zhou M, Zhu L, Zhu G. Flagella and bacterial pathogenicity. J Basic Microbiol. 2013; 53:1–8. [PubMed: 22359233]

Dusenbery DB. Fitness landscapes for effects of shape on chemotaxis and other behaviors of bacteria. J Bacteriol. 1998; 180:5978–5983. [PubMed: 9811657]

Eaton KA, Brooks CL, Morgan DR, Krakowka S. Essential role of urease in pathogenesis of gastritis induced by *Helicobacter pylori* in gnotobiotic piglets. Infect Immun. 1991; 59:2470–2475. [PubMed: 2050411]

Eaton KA, Suerbaum S, Josenhans C, Krakowka S. Colonization of gnotobiotic piglets by *Helicobacter pylori* deficient in two flagellin genes. Infect Immun. 1996; 64:2445–2448. [PubMed: 8698465]

Edelstein A, Amodaj N, Hoover K, Vale R, Stuurman N. Computer control of microscopes using microManager. Curr Protoc Mol Biol. 2010; Chapter 14(Unit14):20. [PubMed: 20890901]

Ferrero RL, Lee A. Motility of *Campylobacter jejuni* in a viscous environment: comparison with conventional rod-shaped bacteria. J Gen Microbiol. 1988; 134:53–59. [PubMed: 3053972]

Frirdich E, Vermeulen J, Biboy J, Soares F, Taveirne ME, Johnson JG, et al. Peptidoglycan LD-carboxypeptidase Pgp2 influences *Campylobacter jejuni* helical cell shape and pathogenic properties and provides the substrate for the DL-carboxypeptidase Pgp1. J Biol Chem. 2014; 289:8007–8018. [PubMed: 24394413]

Georgiades P, Pudney PD, Thornton DJ, Waigh TA. Particle tracking microrheology of purified gastrointestinal mucins. Biopolymers. 2014; 101:366–377. [PubMed: 23955640]

Gray J, Hancock GJ. The propulsion of sea-urchin spermatozoa. J Exp Biol. 1955; 32:802–814.

Greenberg EP, Canale-Parola E. Motility of flagellated bacteria in viscous environments. J Bacteriol. 1977a; 132:356–358. [PubMed: 410784]

Greenberg EP, Canale-Parola E. Relationship between cell coiling and motility of spirochetes in viscous environments. J Bacteriol. 1977b; 131:960–969. [PubMed: 330506]

Hazell SL, Lee A, Brady L, Hennessy W. *Campylobacter pyloridis* and gastritis: association with intercellular spaces and adaptation to an environment of mucus as important factors in colonization of the gastric epithelium. J Infect Dis. 1986; 153:658–663. [PubMed: 3950447]

Howitt MR, Lee JY, Lertsethtakarn P, Vogelmann R, Joubert LM, Ottemann KM, Amieva MR. ChePep controls *Helicobacter pylori* Infection of the gastric glands and chemotaxis in the Epsilonproteobacteria. MBio. 2011; 2

Hyon Y, Powers TR, Stocker R, Fu HC. The wiggling trajectories of bacteria. Journal of Fluid Mechanics. 2012; 705:58–76.

Kanehl P, Ishikawa T. Fluid mechanics of swimming bacteria with multiple flagella. Phys Rev E Stat Nonlin Soft Matter Phys. 2014; 89:042704. [PubMed: 24827275]

Karim QN, Logan RP, Puels J, Karnholz A, Worku ML. Measurement of motility of *Helicobacter pylori*, *Campylobacter jejuni*, and *Escherichia coli* by real time computer tracking using the Hobson BacTracker. J Clin Pathol. 1998; 51:623–628. [PubMed: 9828825]

Lacayo CI, Pincus Z, VanDuijn MM, Wilson CA, Fletcher DA, Gertler FB, et al. Emergence of large-scale cell morphology and movement from local actin filament growth dynamics. PLoS Biol. 2007; 5:e233. [PubMed: 17760506]

Lauga E, Powers TR. The hydrodynamics of swimming microorganisms. Reports on Progress in Physics. 2009; 72:096601.

Lee A, O'Rourke J, De Ungria MC, Robertson B, Daskalopoulos G, Dixon MF. A standardized mouse model of *Helicobacter pylori* infection: introducing the Sydney strain. Gastroenterology. 1997; 112:1386–1397. [PubMed: 9098027]

Li G, Tang JX. Low flagellar motor torque and high swimming efficiency of *Caulobacter crescentus* swarmer cells. Biophys J. 2006; 91:2726–2734. [PubMed: 16844761]

Lieleg O, Vladescu I, Ribbeck K. Characterization of particle translocation through mucin hydrogels. Biophys J. 2010; 98:1782–1789. [PubMed: 20441741]

Liu B, Gulino M, Morse M, Tang JX, Powers TR, Breuer KS. Helical motion of the cell body enhances *Caulobacter crescentus* motility. Proc Natl Acad Sci U S A. 2014; 111:11252–11256. [PubMed: 25053810]

Lowenthal AC, Hill M, Sycuro LK, Mehmood K, Salama NR, Ottemann KM. Functional analysis of the *Helicobacter pylori* flagellar switch proteins. J Bacteriol. 2009; 191:7147–7156. [PubMed: 19767432]

Magariyama Y, Sugiyama S, Muramoto K, Kawagishi I, Imae Y, Kudo S. Simultaneous measurement of bacterial flagellar rotation rate and swimming speed. Biophys J. 1995; 69:2154–2162. [PubMed: 8580359]

Martinez VA, Schwarz-Linek J, Reufer M, Wilson LG, Morozov AN, Poon WC. Flagellated bacterial motility in polymer solutions. Proc Natl Acad Sci U S A. 2014; 111:17771–17776. [PubMed: 25468981]

McClain MS, Shaffer CL, Israel DA, Peek RM Jr, Cover TL. Genome sequence analysis of *Helicobacter pylori* strains associated with gastric ulceration and gastric cancer. BMC Genomics. 2009; 10:3. [PubMed: 19123947]

Mears, P. Doctoral dissertation. University of Illinois; Urbana-Champaign: 2014. Illuminating the relationship between flagellar activity and bacterial swimming.

Montecucco C, Rappuoli R. Living dangerously: how *Helicobacter pylori* survives in the human stomach. Nat Rev Mol Cell Biol. 2001; 2:457–466. [PubMed: 11389469]

Nakamura H, Yoshiyama H, Takeuchi H, Mizote T, Okita K, Nakazawa T. Urease plays an important role in the chemotactic motility of *Helicobacter pylori* in a viscous environment. Infect Immun. 1998; 66:4832–4837. [PubMed: 9746586]

Naughton JA, Marino K, Dolan B, Reid C, Gough R, Gallagher ME, et al. Divergent mechanisms of interaction of *Helicobacter pylori* and *Campylobacter jejuni* with mucus and mucins. Infect Immun. 2013; 81:2838–2850. [PubMed: 23716616]

Ottemann KM, Lowenthal AC. *Helicobacter pylori* uses motility for initial colonization and to attain robust infection. Infect Immun. 2002; 70:1984–1990. [PubMed: 11895962]

Pearson J, Allen A, Venables C. Gastric mucus: isolation and polymeric structure of the undegraded glycoprotein: its breakdown by pepsin. Gastroenterology. 1980; 78:709–715. [PubMed: 6766422]

Peek RM Jr, Crabtree JE. *Helicobacter pylori* infection and gastric neoplasia. J Pathol. 2006; 208:233–248. [PubMed: 16362989]

Pincus Z, Theriot JA. Comparison of quantitative methods for cell-shape analysis. J Microsc. 2007; 227:140–156. [PubMed: 17845709]

Rasband, WS. ImageJ. U.S. National Institutes of Health; Bethesda, Maryland, USA: 1997–2014.

Rodenborn B, Chen CH, Swinney HL, Liu B, Zhang HP. Propulsion of microorganisms by a helical flagellum. Proc Natl Acad Sci U S A. 2013; 110:E338–347. [PubMed: 23319607]

Rogers SS, Waigh TA, Zhao X, Lu JR. Precise particle tracking against a complicated background: polynomial fitting with Gaussian weight. Phys Biol. 2007; 4:220–227. [PubMed: 17928660]

Rolig AS, Shanks J, Carter JE, Ottemann KM. *Helicobacter pylori* requires TlpD-driven chemotaxis to proliferate in the antrum. Infect Immun. 2012; 80:3713–3720. [PubMed: 22802346]

Salama NR, Shepherd B, Falkow S. Global transposon mutagenesis and essential gene analysis of *Helicobacter pylori*. J Bacteriol. 2004; 186:7926–7935. [PubMed: 15547264]

Schneider WR, Doetsch RN. Effect of viscosity on bacterial motility. J Bacteriol. 1974; 117:696–701. [PubMed: 4204439]

Schrager J, Oates MD. The isolation and partial characterization of a glycoprotein isolated from human gastric aspirates and from extracts of gastric mucosae. Biochim Biophys Acta. 1974; 372:183–195. [PubMed: 4371863]

Schreiber S, Konradt M, Groll C, Scheid P, Hanauer G, Werling HO, et al. The spatial orientation of *Helicobacter pylori* in the gastric mucus. Proc Natl Acad Sci U S A. 2004; 101:5024–5029. [PubMed: 15044704]

Sellers LA, Allen A, Morris ER, Ross-Murphy SB. Mechanical characterization and properties of gastrointestinal mucus gel. Biorheology. 1987; 24:615–623. [PubMed: 3502763]

Sharma CM, Hoffmann S, Darfeuille F, Reignier J, Findeiss S, Sittka A, et al. The primary transcriptome of the major human pathogen *Helicobacter pylori*. Nature. 2010; 464:250–255. [PubMed: 20164839]

Shoesmith JG. The measurement of bacterial motility. J Gen Microbiol. 1960; 22:528–535.

Son K, Guasto JS, Stocker R. Bacteria can exploit a flagellar buckling instability to change direction. Nature Physics. 2013; 9:494–498.

Spagnolie SE, Liu B, Powers TR. Locomotion of helical bodies in viscoelastic fluids: enhanced swimming at large helical amplitudes. Phys Rev Lett. 2013; 111:068101. [PubMed: 23971615]

Sycuro LK, Pincus Z, Gutierrez KD, Biboy J, Stern CA, Vollmer W, Salama NR. Peptidoglycan crosslinking relaxation promotes *Helicobacter pylori*'s helical shape and stomach colonization. Cell. 2010; 141:822–833. [PubMed: 20510929]

Sycuro LK, Rule CS, Petersen TW, Wyckoff TJ, Sessler T, Nagarkar DB, et al. Flow cytometry-based enrichment for cell shape mutants identifies multiple genes that influence *Helicobacter pylori* morphology. Mol Microbiol. 2013; 90:869–883. [PubMed: 24112477]

Sycuro LK, Wyckoff TJ, Biboy J, Born P, Pincus P, Vollmer W, Salama NR. Multiple peptidoglycan modification networks modulate *Helicobacter pylori's* cell shape, motility, and colonization potential. PLoS Pathog. 2012; 8:e1002603. [PubMed: 22457625]

Taylor C, Allen A, Dettmar PW, Pearson JP. Two rheologically different gastric mucus secretions with different putative functions. Biochim Biophys Acta. 2004; 1674:131–138. [PubMed: 15374617]

Terry K, Williams SM, Connolly L, Ottemann KM. Chemotaxis plays multiple roles during *Helicobacter pylori* animal infection. Infect Immun. 2005; 73:803–811. [PubMed: 15664919]

Tsang J, Hoover TR. Requirement of the flagellar protein export apparatus component FliO for optimal expression of flagellar genes in *Helicobacter pylori*. J Bacteriol. 2014; 196:2709–2717. [PubMed: 24837287]

Tsuda M, Karita M, Mizote T, Morshed MG, Okita K, Nakazawa T. Essential role of *Helicobacter pylori* urease in gastric colonization: definite proof using a urease-negative mutant constructed by gene replacement. Eur J Gastroenterol Hepatol. 1994a; 6(Suppl 1):S49–52. [PubMed: 7735935]

Tsuda M, Karita M, Morshed MG, Okita K, Nakazawa T. A urease-negative mutant of *Helicobacter pylori* constructed by allelic exchange mutagenesis lacks the ability to colonize the nude mouse stomach. Infect Immun. 1994b; 62:3586–3589. [PubMed: 8039935]

Volocity 3D Rendering and Image Analyses Program. 2011. Volocity: Improvisation PE. Version 6.1

Wang Y, Roos KP, Taylor DE. Transformation of *Helicobacter pylori* by chromosomal metronidazole resistance and by a plasmid with a selectable chloramphenicol resistance marker. J Gen Microbiol. 1993; 139:2485–2493. [PubMed: 8254319]

Worku ML, Sidebotham RL, Baron JH, Misiewicz JJ, Logan RP, Keshavarz T, Karim QN. Motility of *Helicobacter pylori* in a viscous environment. Eur J Gastroenterol Hepatol. 1999; 11:1143–1150. [PubMed: 10524645]

Wroblewski LE, Peek RM Jr. *Helicobacter pylori* in gastric carcinogenesis: mechanisms. Gastroenterol Clin North Am. 2013; 42:285–298. [PubMed: 23639641]

Yeung AT, Parayno A, Hancock RE. Mucin promotes rapid surface motility in *Pseudomonas aeruginosa*. MBio. 2012; 3

Yoshiyama H, Nakazawa T. Unique mechanism of *Helicobacter pylori* for colonizing the gastric mucus. Microbes Infect. 2000; 2:55–60. [PubMed: 10717541]

Young KD. Bacterial morphology: why have different shapes? Curr Opin Microbiol. 2007; 10:596–600. [PubMed: 17981076]

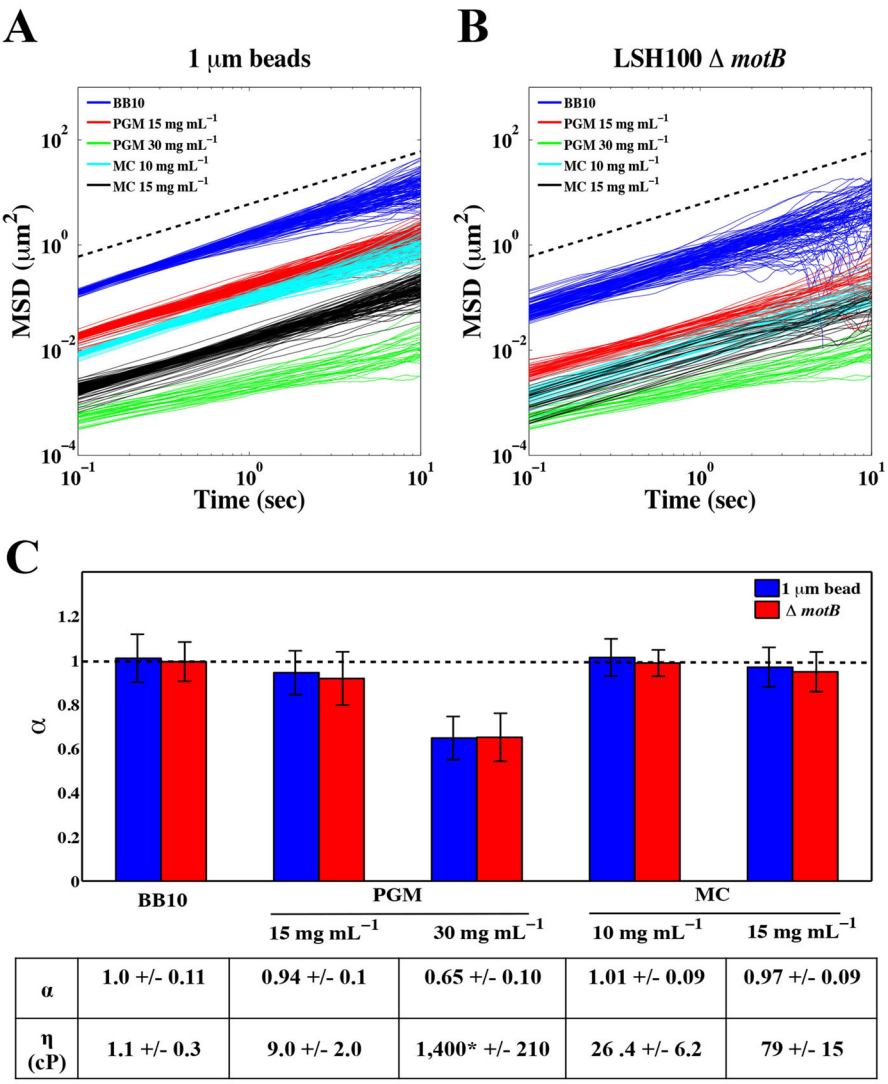

α	1.0 +/- 0.11	0.94 +/- 0.1	0.65 +/- 0.10	1.01 +/- 0.09	0.97 +/- 0.09
η (cP)	1.1 +/- 0.3	9.0 +/- 2.0	1,400* +/- 210	26 .4 +/- 6.2	79 +/- 15

Figure 1. Physiologic concentrations of gastric mucin exhibit solution and gel-like properties

Mean square displacement (MSD, μm^2) values as a function of time (sec) for 1 μm fluorescent particles (A) and LSH100 Δ*motB* bacteria (B) in broth (BB10), PGM (15 mg mL^{-1} and 30 mg mL^{-1}) and MC (10 mg mL^{-1} and 15 mg mL^{-1}) along with (C) Average power of law exponents (α). Average viscosity values (η, cP) and their standard deviations are summarized in the table above (see text for calculation details). All error bars represent standard error and dashed lines represent linear scaling of MSD over time (α=1). *This value is significantly larger compared to the others due to the gel-like nature of PGM at 30 mg mL^{-1}.

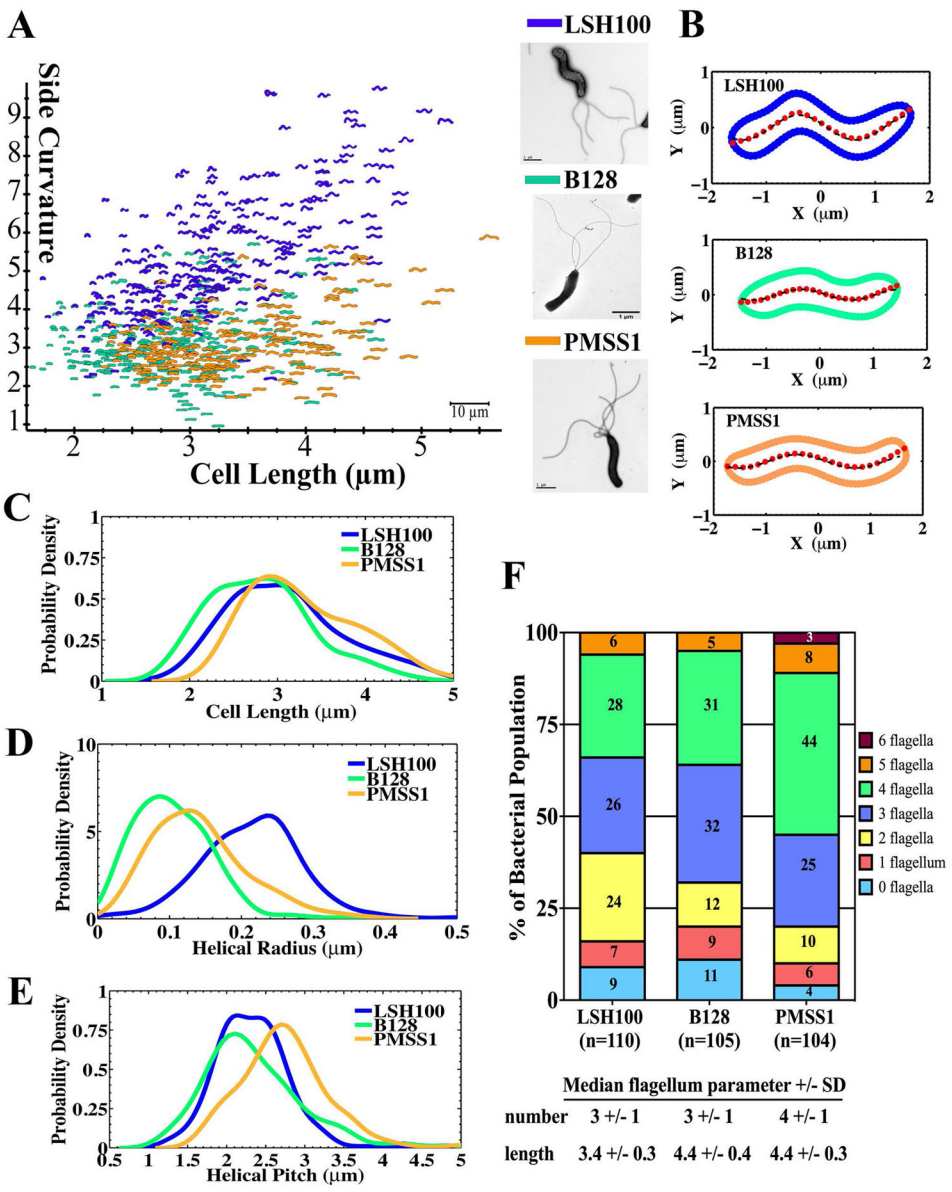

Figure 2. Wild-type *H. pylori* strains display diverse cell shape and flagellum morphologies

(A) Side curvature vs. cell length (μm) for individual bacterial cells imaged using phase contrast microscopy of LSH100 (blue, n=282), B128 (green, n=274), and PMSS1 (orange, n=222) bacteria. Inset panel: TEM images of each. Scale bar = 1 μm. Data combined from two independent cultures for each strain. (B) Representative bacterial centerlines (red dots) for each wild-type strain fitted with a generalized sine function, $y=R\sin(\frac{2\pi}{P}x+\delta)$ (black dashed line); *R*, helical radius; *P*, helical pitch; δ, phase shift term (δ ≈ π for the bacteria shown). (C–E) Smooth histograms of probability density for cell length (μm) (C), helical radius (μm) (D), and helical pitch (μm) (E) of LSH100 (n=262), B128 (n=272), and PMSS1 (n=215) bacteria. (F) Flagellum number counts measured from SEM or TEM images reported as percent of the total bacterial population examined (n=104–110 bacteria).

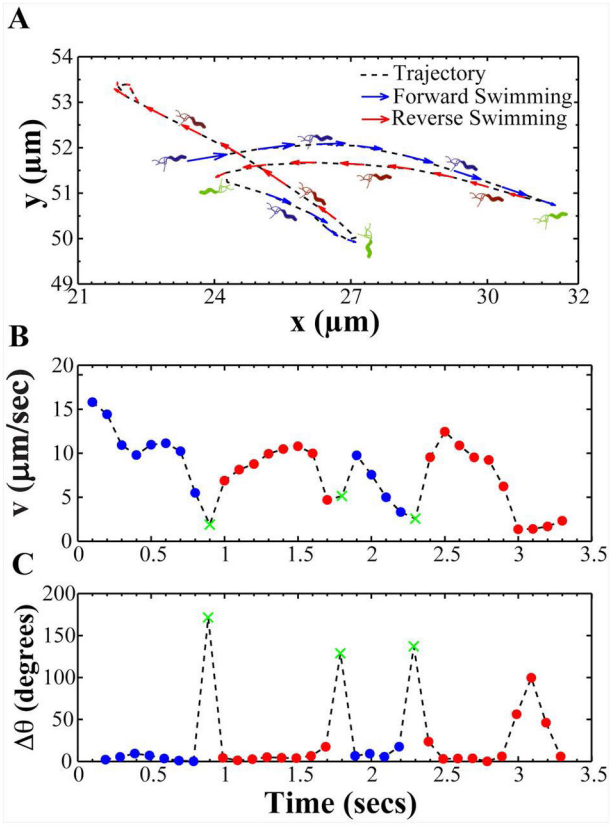

Figure 3. A representative bacterial trajectory depicting the swimming motion of *H. pylori*

(A) A representative bacterial trajectory of *H. pylori* is shown segmented into forward (blue) and reverse swimming directions (red). In our analysis, the direction of swimming observed at the start of the video was considered forward. A reversal in swimming direction (green) was identified when bacteria exhibited a large angle change ($\Delta\theta$) > 110 degrees. Upon a reversal, bacteria were assumed to continue swimming in the reversed direction (red) until another reversal took place. (B) Instantaneous forward and reversal swimming speeds and (C) change in swimming angle ($\Delta\theta$) of the bacterium in panel A over the course of time it was tracked (X (green) denotes reversals in swimming direction).

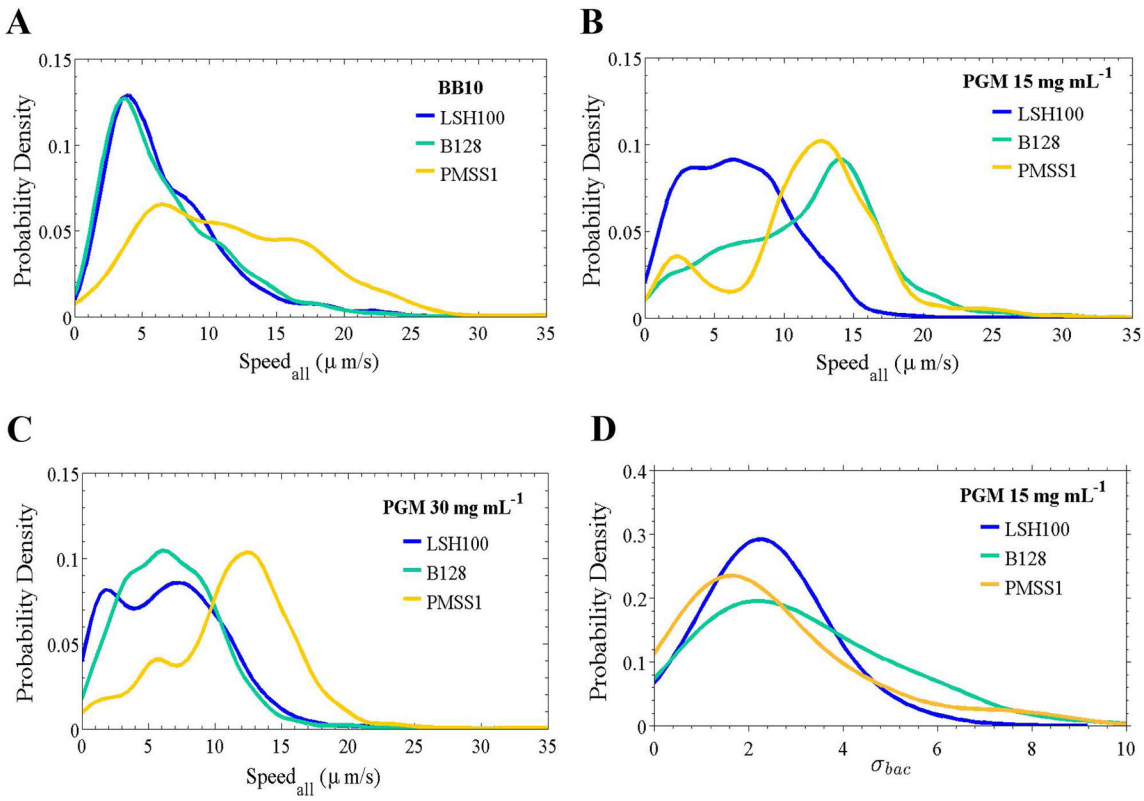

Figure 4. Wild-type *H. pylori* strains display diverse speed profiles and temporal variation in swimming speed

Smooth histograms summarizing speed distributions for all bacteria analyzed ($Speed_{all}$) for LSH100, B128, and PMSS1 bacteria swimming in broth (BB10) (A), in viscous solutions of PGM (15 mg mL^{-1}) (B), and in gel-like PGM solutions (30 mg mL^{-1}) (C). (n=100 bacteria analyzed in each case) (C). Representative data is from one of two or three independent experiments for each strain and the median swimming speeds of each wild-type strain are summarized in Table 2. K-S $p = 0.1100$ for LSH100 vs. B128 in BB10; $p < 0.0001$ for LSH100 vs. PMSS1, and B128 vs. PMSS1 in BB10; and $p < 0.0001$ for LSH100 vs. B128, LSH100 vs. PMSS1, and B128 vs. PMSS1 in viscous PGM media. (D) Smooth histograms summarizing the standard deviation distributions acquired for each individual bacterium's speed trajectory, σ_{bac}, of each wild-type strain in a viscous solution of PGM at 15 mg mL^{-1}. K-S $p = 0.0050$ for LSH100 vs. B128; $p = 0.0314$ for LSH100 vs. PMSS1, and $p = 0.0082$ for B128 vs. PMSS1. K-S $p < 0.05$ was considered significant.

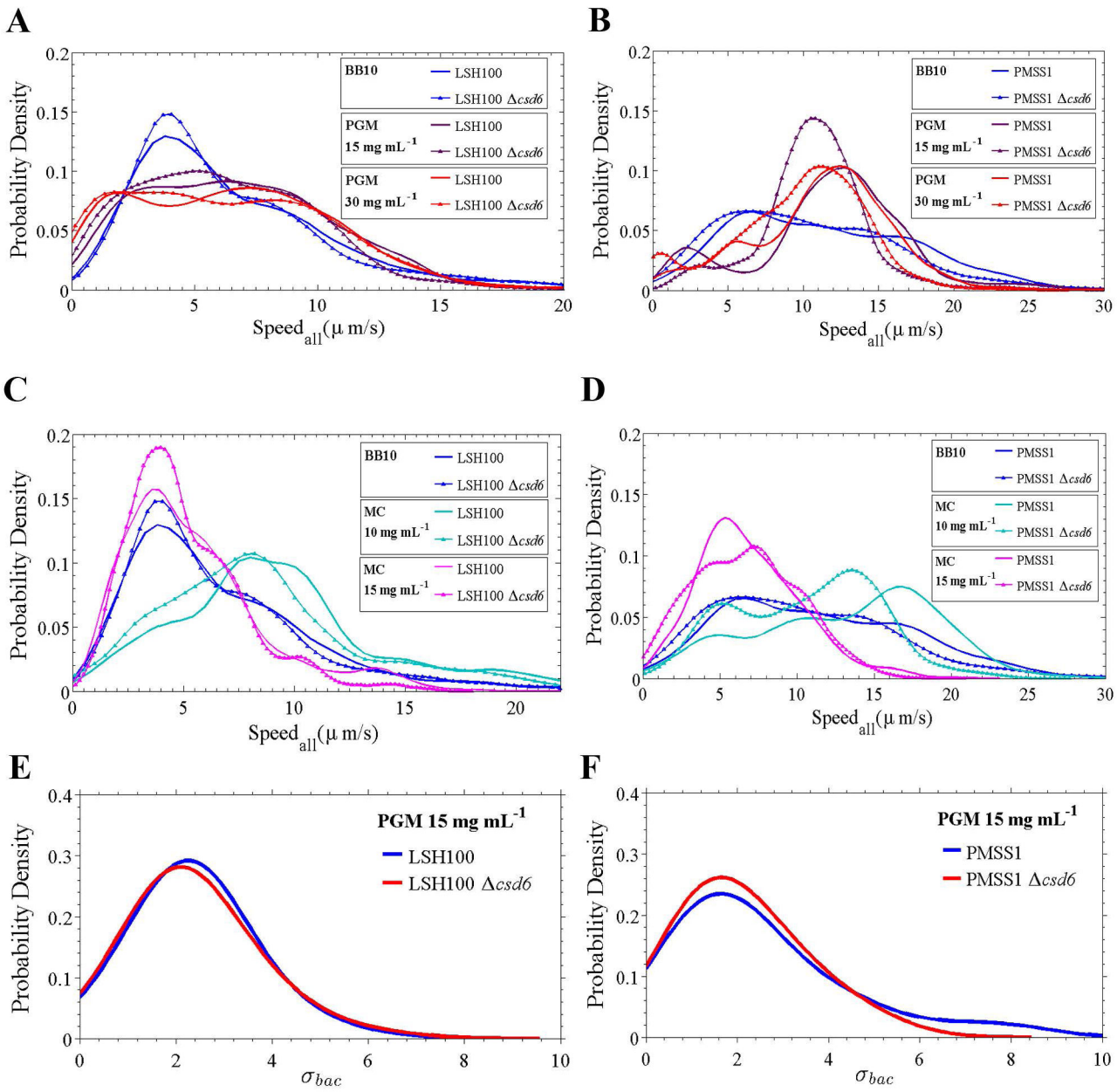

Figure 5. Straight rod mutants show decreased swimming speeds in broth and viscous media

Speed distributions for all bacteria analyzed (Speed$_{all}$) for wild-type and Δ*csd6* isogenic straight rod mutants in broth (BB10) and viscous PGM media (15 and 30 mg mL^{-1}) (A, B), and in broth (BB10) and viscous MC media (10 and 15 mg mL^{-1}) (C, D). One of two or three independent experiments are shown. (E, F) Smooth histograms summarizing the standard deviation distributions acquired for each individual bacterium's speed trajectory, σ_{bac}, of wild-type LSH100 (E) and PMSS1 bacteria (F) as compared to their respective isogenic straight rod mutants in viscous solutions of PGM at 15 mg mL^{-1}. The distributions show similar temporal speed variation profiles between wild-type and straight rod mutants,

where K-S p = 0.44 for LSH100 vs. LSH100 Δ*csd6*, and p = 0.57 for PMSS1 vs. PMSS1 Δ*csd6.*

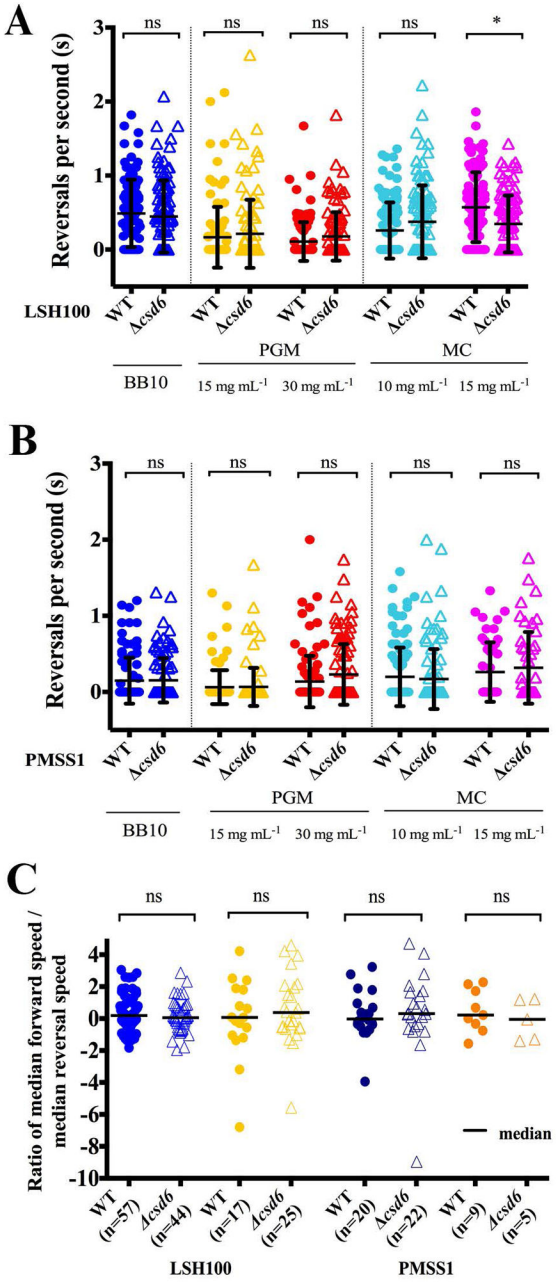

Figure 6. Reversal frequency and ratio of forward to reverse speed are similar across wild-type strains and shape mutants

(A, B) Dot plots summarizing the number of reversals per second of wild-type *H. pylori* strains and isogenic Δ*csd6* straight rod mutants in LSH100 (A) and PMSS1 (B) strains in broth (BB10) and in viscous PGM or MC media. Mean values of reversals per second are shown as bolded black lines and error bars indicate one standard deviation from the mean. Data shown is from one of two or three representative experiments for each strain. (C) Dot plots summarizing individual ratios of median forward swimming speed to median reversal swimming speed acquired for each bacterial cell that reversed and maintained at least 3 instantaneous forward or reversal speed values while swimming in broth or viscous PGM

solutions (15 mg mL^{-1}). Ratios are plotted on a $\log_2$ scale and median values are shown as bolded black lines. All data shown is from the same experiment in Fig. 5. *K-S $p < 0.05$ was considered significant and ns = no significant difference.

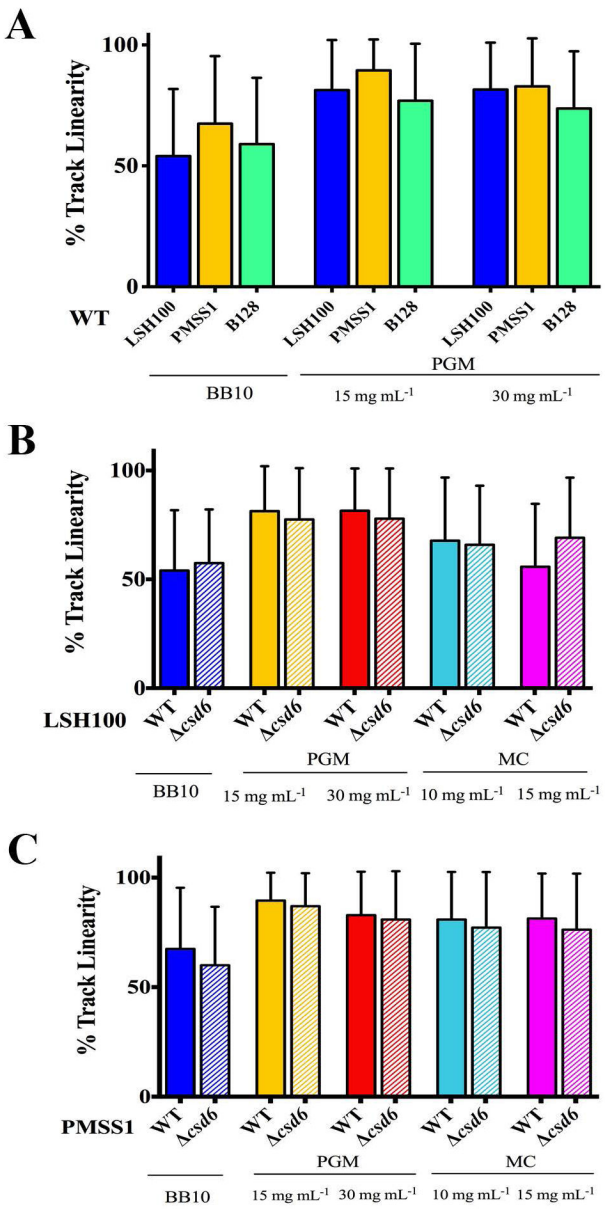

Figure 7. *H. pylori* show increased % track linearity in their swimming trajectories in viscous PGM media, irrespective of cell shape

Bar histograms show cell path trajectory as percent track linearity (%TL) between wild-type *H. pylori* strains (solid bars, A–C) and isogenic Δ*csd6* straight rod mutants (hashed bars, B–C) in LSH100 and PMSS1 strains, as calculated from the ratio of straight-line velocity to curvilinear velocity in broth (BB10) and in viscous PGM or MC media. Error bars represent SD and mean %TL values are summarized in Table 2. Data are from the same experiments shown in Figs 4 and 5.

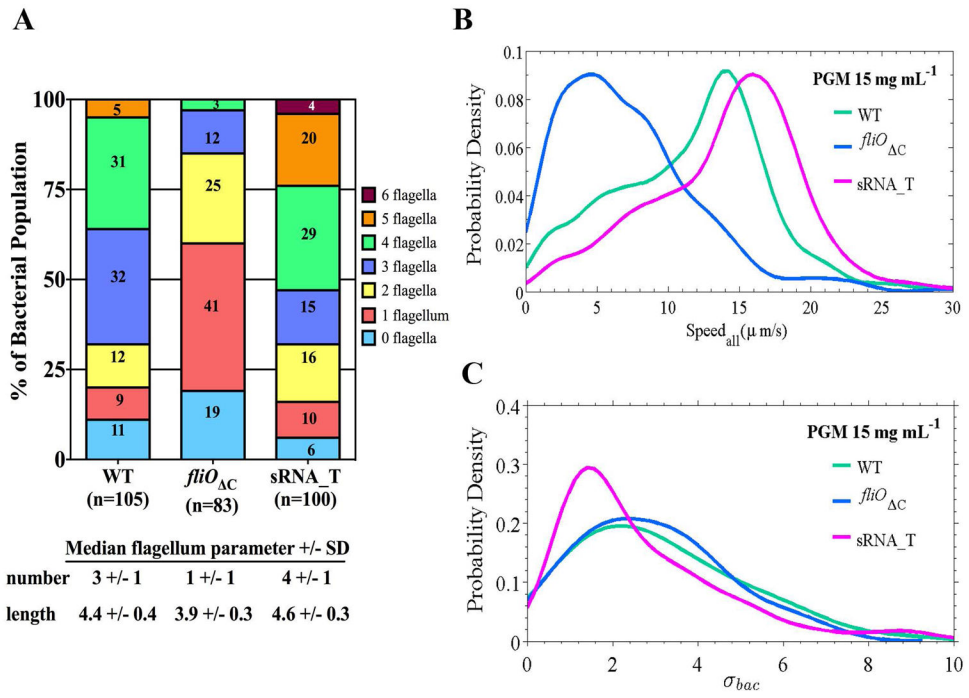

Figure 8. Swimming speed correlates with flagellum number

(A) Individual bacteria were analyzed for the number of flagella from TEM images and are reported as percent of the total bacterial population examined (n=83–105). (B) Speed distributions for all bacteria analyzed ($Speed_{all}$) and (C) distributions summarizing the standard deviation of each individual bacterium's speed trajectory, σ_{bac}, acquired for wild-type B128 and its isogenic flagellar mutants, *fliO*$_{\Delta C}$ and sRNA_T, in viscous solutions of PGM (15 mg mL^{-1}). Representative data is from one of two independent experiments for each strain. The mutant speed distributions are significantly different from wild-type B128, where K-S $p < 0.05$ in each case (see Table 5). No significant difference in temporal speed variation was observed between wild-type B128 and sRNA_T (p=0.10); B128 vs. *fliO*$_{\Delta C}$ (p=0.98); or sRNA_T vs. *fliO*$_{\Delta C}$ (p=0.29).

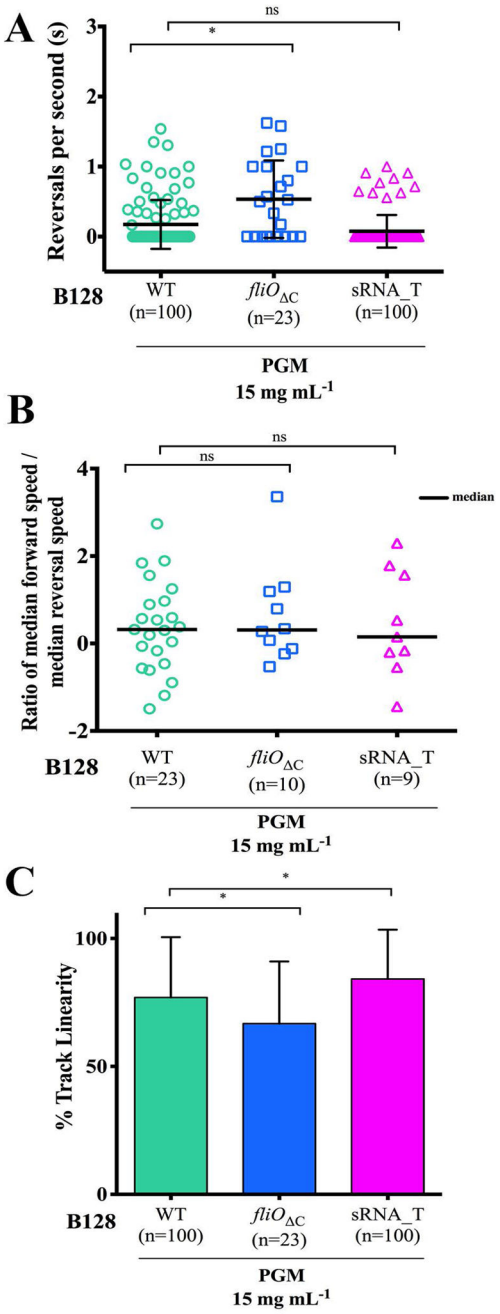

Figure 9. Increased flagellation minimally affects reversal frequency, but increases % track linearity in *H. pylori*

(A) Dot plots summarizing the number of reversals per second acquired for wild-type B128 and isogenic flagellar mutants in viscous PGM solutions (15 mg mL^{-1}). Mean values of reversals per second are shown as bolded black lines and error bars indicate one standard deviation from the mean. The *fliO*$_{\Delta C}$ shows a significant difference to wild-type B128 (K-S, p = 0.0114). (B) Dot plots summarizing individual ratios of median forward swimming speed to median reversal swimming speed acquired for each bacterial cell swimming in PGM (15 mg mL^{-1}). Ratios are plotted on a $\log_2$ scale and median values are shown as

bolded black lines. (C) Bar histograms showing % track linearity (%TL) for wild-type B128 and isogenic flagellar mutants in PGM (15 mg mL^{-1}). Error bars show one standard deviation from the mean and mean %TL values are summarized in Table 5. *K-S $p < 0.05$ was considered significant and ns = no significant difference.

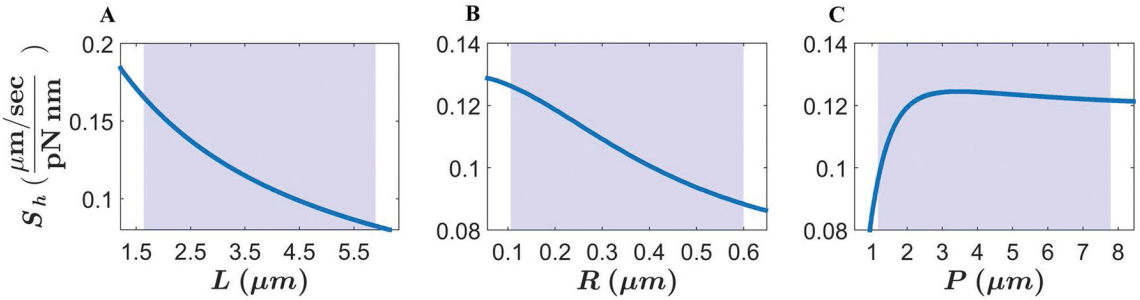

Figure 10. Resistive force theory model predicts that variation in helical body length (*L*), helical radius (*R*), and helical pitch (*P*) alter *H. pylori's* shape factor, S_h

Calculated shape factor (S_h) for a bacterium with helical cell body shape. In each plot, the dependence of S_h is shown for a single cell body parameter L (A), R (B), or P (C) while keeping the other two parameters constant. The parameters that were not varied were maintained at a cell length L = 3.1 μm; helical pitch P = 2.5 μm; helical radius R = 0.15 μm; cell diameter D = 0.56 μm; flagellum length l = 4.1 μm; flagella pitch p = 1.58 μm; flagella helical radius r = 0.14 μm; and flagella bundle thickness d = 0.07 μm. These are the average helical cell body or flagella parameters from the wild-type *H. pylori* strains LSH100, B128, and PMSS1. The blue shaded regions represent the range (min to max) of the cell shape parameters observed experimentally for LSH100, B128, PMSS1, and the B128 sRNA_T mutant (Fig. 2 and Fig. S7).

Table 1

Average cell body and helical parameters of wild-type *H. pylori* strains.

Strain	Average cell body parameters from CellTool[a]				Average helical parameters[b]		
	n	Cell length (μm)	Side Curvature	Cell diameter (μm)	n	Helical radius (μm)	Helical pitch (μm)
LSH100	282	3.17	5.26	0.55	262	0.22	2.3
B128	274	2.82	3.08	0.58	272	0.10	2.4
PMSS1	222	3.33	3.10	0.57	215	0.14	2.8

[a]Cell body parameters acquired from CellTool.

[b]Helical parameter measurements acquired from fitting centerlines to a sinusoid.

Table 2

Speeds for wild-type bacteria and straight rod mutants swimming in broth and viscous media.

Solution	Strain		n	Inst. values	v_{avg} (μm/s)	v_m (μm/s)	v_{max} (μm/s)	σ	K-S p-value[c]	% reduction to v_m relative to WT
BB10		**B128**	99	2105	6.6	5.5	28.0	4.3		
	LSH100	**WT**	100	2538	6.8	5.7	48.0	4.7	0.0955	7%
		Δ*csd6*	100	2058	6.5	5.3	30.1	4.1		
	PMSS1	**WT**	100	1975	11.6	10.8	49.2	6.3	<0.0001	11%
		Δ*csd6*	100	1930	10.5	9.6	38.8	6.0		
PGM[a] 15 mg mL^{-1}		**B128**	100	2112	11.7	12.5	36.6	5.5		
	LSH100	**WT**	100	3325	6.7	6.5	29.1	3.8	<0.0001	11%
		Δ*csd6*	100	3886	6.2	5.8	22.8	3.6		
	PMSS1	**WT**	100	2073	11.8	12.2	39.3	5.3	<0.0001	11%
		Δ*csd6*	100	2550	10.7	10.8	28.4	3.6		
PGM 30 mg mL^{-1}		**B128**	100	2752	6.7	6.5	41.9	3.7		
	LSH100	**WT**	100	2790	6.6	6.4	30.1	4.2	0.0005	8%
		Δ*csd6*	100	2951	6.3	5.9	33.3	4.2		
	PMSS1	**WT**	100	2224	11.3	11.8	34.8	4.7	<0.0001	13%
		Δ*csd6*	100	2276	9.7	10.3	24.8	4.4		
MC[b] 10 mg mL^{-1}	**LSH100**	**WT**	100	2076	9.5	8.8	46.1	5.2	<0.0001	10%
		Δ*csd6*	100	2151	8.6	7.9	39.4	5.0		
	PMSS1	**WT**	100	1874	13.2	14.2	32.2	5.8	<0.0001	21%
		Δ*csd6*	100	2251	10.6	11.2	24.2	4.6		
MC 15 mg mL^{-1}	**LSH100**	**WT**	100	3194	5.5	4.8	26.1	3.3	<0.0001	6%
		Δ*csd6*	100	3544	5.1	4.5	16.6	2.6		
	PMSS1	**WT**	48	965	6.9	6.4	20.6	3.3	0.0104	NR[d]
		Δ*csd6*	48	1201	6.8	6.8	17.9	3.4		

[a] PGM: Purified gastric mucin at pH 6.0.

[b] MC: Methylcellulose.

[c] For K-S tests used to compare WT to mutant cumulative distributions of swimming speeds, p-values < 0.05 are considered significant.

d_{NR}: No reduction.

Table 3

Fraction of immobile bacteria in broth and viscous PGM media.

Strain		BB10		PGM[a] 15mg mL^{-1}		PGM 30 mg mL^{-1}	
		n	% immobile[b]	n	% immobile	n	% immobile
LSH100	**WT**	977	20	536	24	820	50
	Δ*csd6*	494	21	546	30	456	52
Increase in % immobile bacteria relative to WT		5%		25%		4%	
PMSS1	**WT**	558	10	330	15	456	38
	Δ*csd6*	371	13	328	21	504	51
Increase in % immobile bacteria relative to WT		30%		40%		34%	

[a]PGM: Purified gastric mucin at pH 6.0.

[b]Bacteria exhibit displacements < 0.3 μm (MSD < 0.1 μm^2).

Table 4

Median flagellum parameters of wild-type *H. pylori* and isogenic straight rod mutants.

Strains	Median flagellum parameter[a] +/− SD[b]			
	n	Flagellumnumber	n	Flagellum length (μm)
LSH100	110	3 +/− 1	15	3.4 +/− 0.3
LSH100 Δ*csd6*	109	3 +/− 1	15	3.3 +/− 0.4
PMSS1	104	4 +/− 1	15	4.4 +/− 0.3
PMSS1 Δ*csd6*	105	4 +/− 1	15	4.2 +/− 0.2

[a] Flagellum number counts were acquired from SEM images and flagellum length measurements were acquired from TEM images.

[b] Standard Deviation (SD).

Table 5

Speeds, percent track linearity, and the fraction of immobile wild-type bacteria and flagellar mutants in viscous PGM solutions (15 mg mL^{-1}).

	PGM[a] 15 mg mL^{-1}		
	WT B128	**B128 *fliO*$_{\Delta C}$**	**B128 sRNA_T**
n	100	23	100
Inst. values	2112	553	1673
v_{avg} (μm/s)	11.7	7.2	14.2
v_m (μm/s)	12.5	6.3	14.9
v_{max} (μm/s)	36.6	29.8	40.5
σ	5.5	4.8	5.6
K-S p-value[b]	<0.0001		<0.0001
% reduction to v_m relative to WT	50%		19% increase
Average %TL	77%	67%	84%
K-S p-value[b] for % TL	0.041		0.037
n	461	270	440
%Immobile[c]	36%	82%	14%
%clumps[d]	0.43%	31%	0.68%

[a] PGM: Purified gastric mucin at pH 6.0.

[b] For K-S tests used to compare WT to mutant cumulative distributions of swimming speeds and percent track linearity (%TL), p-values < 0.05 are considered significant.

[c] Fraction of immobile bacteria in viscous PGM solutions. Bacteria exhibit displacements < 0.3 μm (MSD < 0.1 $μm^2$).

[d] Fraction of clumped bacteria in viscous PGM solutions.

Table 6

Comparison of experimental median speeds in PGM 15 mg mL^{-1} and predictions of Resistive Force Theory model implementations.

Strain	Median speed in PGM[a] 15 mg mL^{-1}(μm/s)	S_h[b] +/− SE[c]	S_hN_f[d] +/− SE[b]
LSH100	6.5	115 +/− 10	345
PMSS1	12.2	120 +/− 7	480
B128	12.5	132 +/− 8	396
B128 sRNA_T	14.9	116 +/− 8	464

Strains compared	Ratio of median speed in PGM[a] 15 mg mL^{-1}	Ratio of S_h +/− SE[b]	Ratio of S_hN_f +/− SE[b]
sRNA_T/B128	1.2	1.9 +/− 0.1	1.2 +/− 0.1
sRNA_T/PMSS1	1.2	1.0 +/− 0.1	1.0 +/− 0.1
B128/PMSS1	1.0	1.1 +/− 0.1	0.8 +/− 0.1
LSH100/PMSS1	0.5	1.0 +/− 0.1	0.7 +/− 0.2

[a] PGM: Purified gastric mucin at pH 6.0.

[b] SE: Standard error.

[c] S_h: Shape factor.

[d] S_hN_f: the product of shape factor and median flagellum number.